NEXALUS
COOLING THE CLOUD

Present and future thermal interface materials for electronic devices

Kafil M. Razeeb[a], Eric Dalton[b], Graham Lawerence William Cross[c] and Anthony James Robinson[d,e]

a Tyndall National Institute, University College Cork, Cork, Ireland
b Stokes Laboratories, University of Limerick, Limerick, Ireland
c School of Physics, CRANN Nanotechnology Institute, Trinity College Dublin, Dublin 2, Ireland
d Department of Mechanical & Manufacturing Engineering, Trinity College Dublin, Dublin 2, Ireland
e CONNECT, Dunlop Oriel House, Trinity College, Dublin, Ireland

Abstract

Packaging electronic devices is a growing challenge as device performance and power levels escalate. As device feature sizes decrease, ensuring reliable operation becomes a challenge. Ensuring effective heat transfer from an integrated circuit and its heat spreader to a heat sink is a vital step in meeting this challenge. The projected power density and junction-to-ambient thermal resistance for high-performance chips at the 14 nm generation are >100 Wcm^{-2} and <0.2°C W^{-1}, respectively.

The main bottleneck in reducing the net thermal resistance are the thermal resistances of the thermal interface material (TIM). This review evaluates the current state of the art of TIMs. Here, the theory of thermal surface interaction will be addressed and the practicalities of the measurement techniques and the reliability of TIMs will be discussed. Furthermore, the next generation of TIMs will be discussed in terms of potential thermal solutions in the realisation of Internet of Things.

Keywords: Thermal interface materials; solder; carbon structure; polymer composite; thermal conductivity; thermal resistance

1. Introduction

Thermal interface material or TIM can be defined as any material that is applied between the interfaces of two components to enhance the thermal coupling between these devices.

Usually, TIM is used between a heat generating device (e.g. microprocessor, photonic integrated circuits, etc.) and a heat dissipating device (e.g. heat sink) to remove the heat from the component. The effective transfer/removal of heat from a semiconductor device is crucial to ensure reliable operation and to enhance the lifetime of these components. Microscopic surface roughness and non-planarity of the IC/heat spreader and heat sink surfaces result in asperities between the two mating surfaces. These asperities prevent the two solid surfaces from forming a thermally perfect contact due to the poor thermal conductivity of air that exists in the gaps between two mating surfaces [1]. TIMs are therefore used to provide an effective heat conduction path between the solid surfaces due to their conformation (under pressure) to surface roughness and reasonably high thermal conductivity [2].There are different types of TIMs available both commercially as well as in the research and development phase. From an application point of view, the commercially available TIMs are usually based on different types of filler materials in a polymer matrix or are solder based. In recent years carbon-based TIMs have also been widely investigated. Broadly speaking, these materials can be divided into three different classes: Carbon-based, metal/solder and filler-based TIMs. These again can be divided into solder, alloys, metallic foils, different types of carbon structures (carbon nanotube, graphene, graphite, etc.) and polymer (grease, phase change materials, adhesives, elastomer, and thermoplastic, etc.) based TIMs.

To the best of our knowledge, a comprehensive review on TIMs is still missing (except the recent complementary review by Hansson et al. [3]), where the last review was done in 2013 on 'Reliability of thermal interface materials' [4] and in 2012 on 'Characterization of nanostructured thermal interface materials – A review' [5]. Thereby, it is envisaged that a thorough review on this topical area would benefit new researchers in this area as well as application engineers who are looking for the right TIMs for their specific application. It is intended that this review will cover the last decade or so of research in the area with particular focus on recent trends and technologies.

This review is divided into the following section: TIM market, theoretical concept of TIMs and associated phenomena, measuring thermal performance of TIM, different types of TIMs and concludes with a summary and outlook. It is hoped that this review will enhance the understanding of the present status of TIM technology and help researchers and practitioners understand the gaps and opportunities which will allow them to direct their future research and development to meet the requirements of thermal management of next-generation electronic and photonic devices.

2. TIM market

Future electronics and photonics systems will face overheating problems associated with excess heat as long as these systems are not monolithic, but are built using different materials, e.g. semiconductors, metals, ceramics and polymers. In the vision of the Internet of Things, the rise in power densities due to miniaturisation in electronic and photonics systems will make effective heat removal a critical issue for the progress in communication, information, energy harvesting and lighting technologies. The fundamental problem will be the reduced performance, reliability and lifetime of these electronic devices due to excess heat, which cannot be removed without implementing an effective thermal path between heat generating device (e.g. microprocessor) and the heat removing component such as heat sink. Therefore, the requirement of effective thermal interface materials within 'stacked' electronics packages is vital to ensure reliable and safe operation.

The TIM market is now continuously monitored by major market research firms such as BCC Research in Massachusetts, USA [6] and IDTechEx of London, UK [7]. While the detailed market information is proprietary, major trends are provided in free executive summaries [8–10].

The TIM market is defined by the spectrum of products discussed in this review including polymer and polymer composite-based gels, greases, pads, and adhesives, various metal-based films, phase change materials, as well as emerging technologies such as carbon-based materials. Polymer-based TIMs dominate with over 80% of the market today, with the rest forming a small but more rapidly growing set of emerging solutions.

TIMs are used in a multitude of industrial sectors identified as computers, consumer devices, telecommunication infrastructure, LED lighting products, renewable energy, automotive, military/ industrial equipment, and medical equipment. The strongest growing areas are anticipated in LED, thin film photovoltaic, consumer, and medical devices, with slower growth in more mature computer, military, and automotive areas. These are led by new technologies such as phase change and metallic TIMs especially for high-temperature applications, followed by adhesives in more traditional approaches. The LED application is of particular note, as it is expected to be the fastest growing and dominant TIM application. Elastomeric pads are used here, and thus are expected to be the dominant form of TIM.

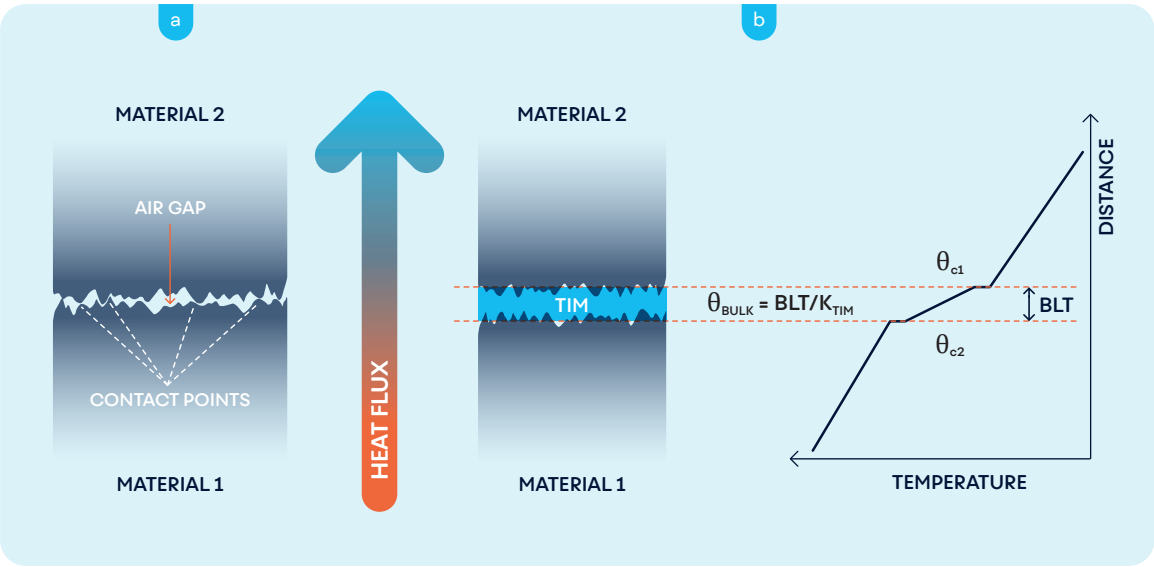

Fig 1. (A) Schematic showing the real area of contact of a joint formed by two rough surfaces; (B) sketch representing a TIM in the real application scenario. Adapted from Prasher [14]. Copyright 2016, IEEE. Reprinted with permission.

3. The theoretical concept of thermal interface materials and its associated phenomena

Without thermal interface material, if two nominally flat and smooth solid surfaces are joining together to form a dry joint [11], roughness on both surfaces can limit the actual area of contact between the two solids to a small percentage (about 1–2%) of the apparent contact area [12] as is depicted in Figure 1(a). If we neglect the heat transfer by radiation between the surfaces, the heat flux through this interface flows by two different heat conduction paths: solid-to-solid conduction through the contact points and conduction through the air trapped between the area of non-contact, which is a poor thermal conductor compared to the solid materials. These two different heat conduction paths limit the heat transfer from one surface to another and has been defined as thermal contact resistance. In order to decrease the temperature drop across the junction, one needs to reduce this thermal contact resistance. To do so, the air gap formed by the mating surfaces must be replaced by a material with higher thermal conductivity than that of the air, which is known as the TIM. Figure 1(b) shows the total thermal resistance due to the TIM insertion (θ_{TIM}) between the two mating surfaces, which can be formulated as follows [13]:

$$\theta_{TIM} = \frac{BLT}{k_{TIM}} + \theta_{c1} + \theta_{c2} \quad (1)$$

where k_{TIM} is the thermal conductivity, BLT is the bond line thickness and θ_{c1} and θ_{c2} represent the contact resistances of the TIM with the two bonding surfaces. Since the main objective of thermal management in electronic packaging is the effective removal of heat from the semiconducting device to the ambient, the total thermal resistance from the junction-to-ambient (θ_{ja}) has to be reduced: the lower the thermal resistance, the lower the temperature drop from the heat generating device to the ambient.

Figure 2 shows representative schematics of two microprocessor package assemblies used in a real application scenario of electronics cooling and the associated thermal resistances. However, many other variants exist [15]. Figures 2(b,d) show that the heat transfer through the complete assembly involves three major stages (along with the respective thermal resistances) [16]:

- Heat transfer within the device package (θ_{jc}).
- Heat transfer from the package to a heat sink (θ_{cs}).
- Heat transfer from the heat sink to the ambient environment (θ_{sa}).

In reducing θ_{ja}, the main bottlenecks are the inter-facial resistances between the package and the heat sink [14]. These resistances are due to the mating surfaces between the package and the heat sink, which in the real application scenario are generally neither fully conforming nor smooth enough and thus lead to a significant increment of thermal contact resistance. Therefore, the thermal management within the area of the chip is a relevant issue. Table 1 summarises the ongoing challenges related to widely adopted air-cooling technology to minimise the junction-to-case thermal resistance.

Similar to the surface roughness of the heat sink and generating devices, the conformity of the thermal interface materials under certain pressure plays a major role in reducing the thermal contact resistance. In this regard, soft material is preferable as an interface material, which can conform to the roughness of the two mating surfaces under reasonable pressure (~200 kPa). Apart from the contact thermal resistance, the bulk thermal resistance (θ_{bulk}) of the interface material is important in defining the overall effectiveness of the material which can be defined in terms of intrinsic thermal conductivity (k_{TIM}) of the material.

Thermal conductivity and thermal resistance

The overall thermal resistance of the TIM also depends on the intrinsic thermal conductivity which is the property of the constituent materials to conduct heat and can be defined in terms of Fourier's law for one-dimensional heat conduction under steady state conditions by:

$$k = \frac{Q}{A}\frac{\Delta x}{\Delta T} \quad (2)$$

where Q is the heat flow (W), A is the surface area (m^2), ΔT is the temperature difference between two surfaces (K), Δx = BLT = thickness of the thermal interface material (m) and k is the thermal conductivity ($Wm^{-1}K^{-1}$).

Thermal resistance R is defined from the above equation as

$$R = \frac{\Delta T}{Q} = \frac{\Delta x}{kA}\left(KW^{-1}\right) \quad (3)$$

whereas thermal resistance for a unit area is defined as

$$\theta = RA = \frac{\Delta x}{k}\left(m^2KW^{-1}\right) \text{ or } \left(cm^2KW^{-1}\right) \quad (4)$$

Physical considerations

The physical aspects of the thermal interface are a multi-disciplinary problem bringing together contact mechanics, tribology, rheology, heat transport and percolation. At an interface, the core transport problem starts with the propagation of heat carriers such as phonons and electrons across a boundary region physically different from the bulk.

For polycrystalline materials, this problem is actually already manifest in the bulk itself across internal grain boundaries, although these boundaries generally have a small impact relative to a perfect crystal as long as they are not too large in number (e.g. the material is not nanocrystalline) and minimally perturb the bulk structure:

For example in diamond at room temperature, thermal conductivity drops with grain size only below about 5µm, where it falls from over 2000 Wm^{-1} K^{-1} to a few Wm^{-1} K^{-1} at the ultra-nanocrystalline scale of a few nanometre grain size [22]. The formation of high quality, large area junctions between dissimilar bodies is largely the domain of heterogeneous integration of compound semiconductors [23], where techniques include epitaxial growth, wafer bonding, and nanomembrane transfer.

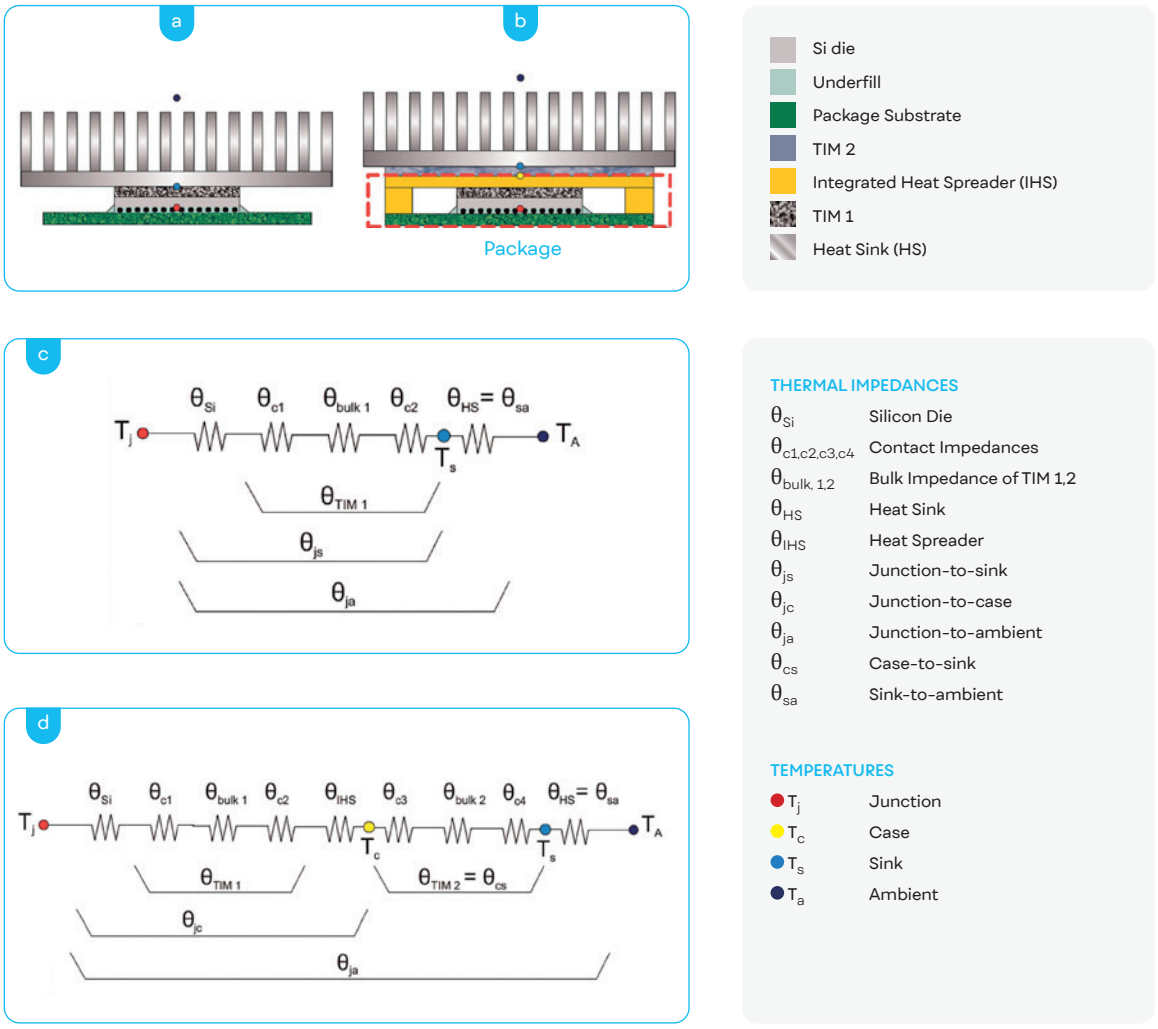

Fig 2. (a, b) shows two sketches of a microprocessor package assembly used in a real application scenario of electronics cooling, respectively, for past and more recent desktop applications. (c, d) The superimposition of different layers of materials in order to build the assembly leads to a creation of a thermal resistance network. Adapted from Refs. [11,14,17–20]. (Note: thermal impedance and resistance tend to be used interchangeably.) Reprinted with permission.

Boundary resistance at these high-quality junctions are studied by a number of advanced techniques such as time domain thermoreflectance, and are affected by nanoscale roughness, disorder, dislocations and other effect of the joining process (see Hopkins [24] for recent review). For example, recent investigations have explored the effect of pressure and crystal orientation, and surface chemistry at the aluminium/diamond interface formed by deposited Al growth, showing up to a fivefold decrease in boundary resistance for oxygen vs. hydrogen termination [25]. For the more common oxygen terminated surface, typical values range from 1.4×10^{-4} to 5×10^{-5} cm^2 KW^{-1} for the [100] vs. [110] diamond face at low pressure [26], decreasing to a common value of 3×10^{-5} cm^2 KW^{-1} at high pressures above 20 GPa. For a mechanically formed interface, the lowest thermal boundary resistance claimed to date [27] is between a [100] single crystal silicon membrane adhered by van der Waals forces to a bulk [100] single crystal oriented in the same crystallographic direction to eliminate acoustic mismatch. A value of 2.8×10^{-5} cm^2 KW–1 was reported for mating of a hydrogen-terminated to an oxide-terminated surface. In this case, contacts of chemically etched surfaces were formed by a dry transfer method followed by annealing, with no external pressure applied.

Thermal resistance	Thermal management challenge
Junction-to-case	IC-level cooling
	Package architecture development
	Interface thermal contact resistance reduction
Case-to-heat sink	Interface thermal contact and TIM bulk resistance minimisation
Heat sink to ambient	Advanced heat sink manufacturing technologies
	Improvement of heat spreading technologies
	Integration of hybrid cooling solutions
	Aerodynamic fan performance improvement
	Airflow optimisation
	Heat sink surface fouling minimisation
	Sustainability

Table 1. Air-cooling solutions: thermal management key areas for improving the heat removal from the silicon die to the heat sink [21] Reprinted with permission..

The introduction of larger scale surface roughness, waviness, damage, and contamination, generally as a by-product of the machining, polishing, casting and handling methods used for device packaging and integrating other thermal hardware such as heat pipes, heat spreaders and heat sinks, severely degrades the thermal interface performance relative to the values discussed above. For example, the performance of the mating of bare machined metal surfaces was reviewed recently by Dou et al.. [28] and their summary comparison is reproduced in Figure 3 (the performance regime of commercial TIMs as well as the limit of smooth silicon membranes for an estimated range of surface-force adhesion pressure modulated by atomic-scale roughness are also shown for comparison).

At pressures relevant to most thermal interface assembly of 100s of kPa, it can be seen that machined surfaces thermal contact resistance ranges over the region of 1–10 cm^2 KW^{-1} for roughness (as measured by the standard parameter R_a) ranging from the sub to multiple micrometre level. Overall, these real interfaces exhibit a contact resistance five orders of magnitude higher than pristine interfaces. The role of roughness induced air-filled gaps in the thermal conductance degradation is strongly suggested by the observed resistance dependence on manufactured surface roughness: A resistance drop of about one order in magnitude is observed for an order of magnitude drop in roughness R_a going from 2–0.2 µm. Assuming, very roughly, a square relation on increase of contact area with the linear roughness parameter, a further drop to nanometre scale roughness of the bonded semiconductor surfaces discussed above gives a four orders of magnitude drop in contact resistance, or about 1×10^{-4} cm^2 KW^{-1} which is well within the range observed for wafer-bonded and other more pristine interfaces. Further, applied clamping pressures to 10 MPa and above can reduce the resistance by a factor of three or four, although there is significant scatter in the accumulated data. This is consistent with rapid area increase by deformation. These relative resistance decreases are far greater than for complete, void-less contacts, even though the pressure change is much smaller [26].

The underlying principle of all TIMs is thus to address the contact area problem. They replace air-filled microscopic roughness voids by deforming under permitted assembly pressures. The deformability requirement leads to their most fundamental engineering trade-off: low mechanical shear strength to allow shape change and conformal interfacial contact implying poor thermal conductivity, generally about two orders of magnitude lower than the packaging and thermal management components they mate together. The problem does not stop there however, because the global geometry and mechanics of thermal interface forming is very poor at generating the shear stress necessary for flow processes. The high aspect ratio geometry of TIM deformation is known in mechanics as a 'poker-chip' geometry and is found in tack testing [29] (under tensile loads), nanoimprint [30,31], etc.

For example, in viscoelastic solids, i.e. materials with a permanent shear modulus as well as viscous nature, this geometry implies a rapidly increasing hydrostatic pressure component of the total stress with Poisson's ratio, leading to a purely hydrostatic deformation in the incompressible limit at long times. While this does not affect microscale cavity filling due to the sharp, local geometry there, it does lead to the problem of the bond line thickness. This is a parasitic global effect whereby the inability to thin the TIM material leaves it to occupy a large gap between the mating surfaces despite the fact that it is able to fill local voids. Thus, despite the fact that TIM materials are only two orders of magnitude worse thermal conductors than metals, their ability to restore the 1×10^{-4} cm^2 KW^{-1} levels of conductance of pristine interfaces is hampered by the presence of the bond line. A typical bond line thickness of 50 µm for a high performance 5 Wm^{-1} K^{-1} paste sets an effective interface resistance of 1 cm^2 KW^{-1} due to the bulk matter of the TIM.

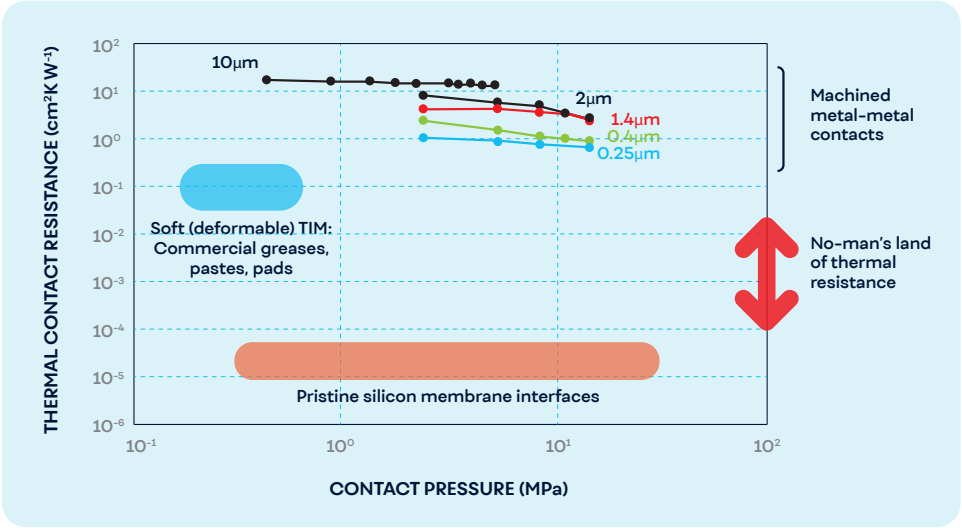

Fig 3. Range of contact thermal resistance from bare machined metal contacts showing effect of surface roughness and contact pressure to general effect of all commercial TIMs (upper oval region) which leave a 'no-man's land' of thermal contact resistance compared to pristine silicon membrane contact under van der Waals forces (lower oval region). Adapted from Dou et al. [28]. Copyright 2016, Elsevier. Reprinted with permission.

Improvements to the current generation of deformable commercial TIM materials come from reduction in the bond line thickness, essentially given by deformability, and/or increases in the bulk thermal conductivity of the TIM. The question of the interfacial thermal resistance of the TIM material itself to the mating surfaces appears to only become important in high-performance TIMs like carbon-nanotube forests.

The aspects discussed above are well summarised by Equation (1) above for the total thermal contact resistance. Reviews of the fundamental research performed to optimise each parameter in this equation has been given in 2006 by Prasher [32] and, covering the last ten years, Luo et al. [33]. As pointed out by these authors, most research consists of improving k_{TIM} through the use of improved materials and/or fillers to an existing polymer-based carrying matrix.

Work on understanding and improving the BLT and solid–liquid contact resistances, starting with more realistic models of loaded paste flow and capillary physics [34–38], is far more limited. Approaches to modifying TIM deformation during assembly flow through surface patterning have shown how to reduce the BLT from 10s to single micrometres [39–41], as well as improving the distribution of loaded particles [42,43] through both design of hierarchal channels and increased rate of TIM compression. These novel effects are schematically summarised in Figure 4.

Of some interest in recent work is understanding when the solid/liquid interface thermal resistances $u_{c1,c2}$ as found in polymer-based TIMs become more important than the BLT/k_{TIM} term in the total resistance. Luo's group, building off of an modelling approach developed by Hamsaiid et al. [36,37], have tested against aluminium blocks of known roughness with silicon oils and thermal greases [38]. The model, with basis in the widely used flux tube concept of Yovanovich [44] for thermal contact resistance, employs roughness topography approximations of Hamasaiid together with a analysis that balances applied pressure, capillarity pressure, and back pressure of trapped air to determine the mean height of the volume of air trapped in roughness cavities. A detailed mechanical analysis that includes the surface energy of the fluid, its contact angle with the surface, and ideal gas behaviour gives a contact resistance that depends on applied pressure, wetting, surface topography, material thermal conductivity, and temperature. By measuring contact resistance by static technique in symmetric junctions with a range of BLT values and extrapolating to zero thickness, it was found that u_c's had a value around 0.1 cm^2 KW^{-1} for the conditions tested, at the lower limit of most commercial TIM performance.

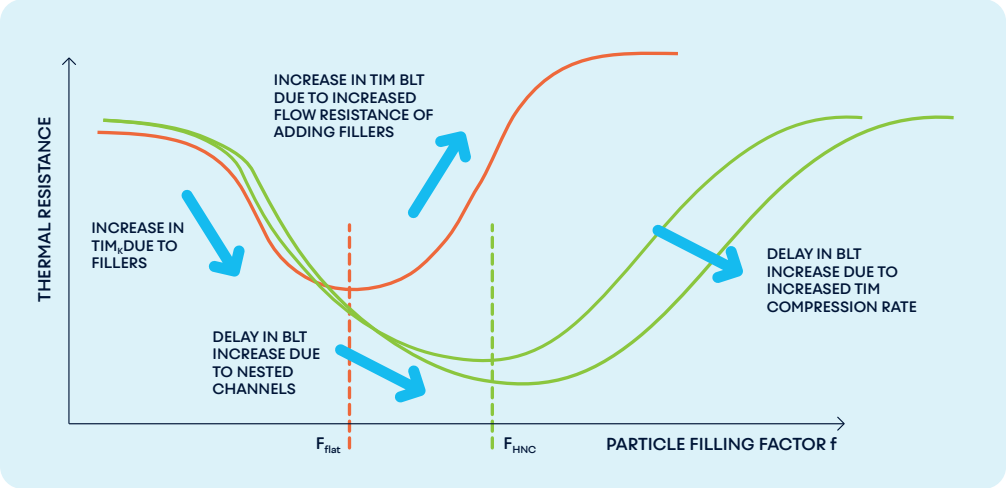

Figure 4. Effect of particle fillers on thermal resistance of TIMs. Micrometre scale hierarchal nested channels (HNC) fabricated in mating surfaces delay onset of bondline thickness (BLT) increase, allowing lower thermal resistance to be achieved. Higher compression rates during TIM bondline forming also improve resistance through improved particle stacking. Adapted from Linderman et al. [37]. Copyright 2016, IEEE. Reprinted with permission.

4. Measuring thermal performance of TIMs

The effectiveness of a TIM is best quantified in terms of its area averaged thermal resistance (RA) when compressed between two heat transfer surfaces [1]. For TIM1 applications, the heat transfer surfaces may be the semiconductor (representing a die) and metal or ceramic (representing a heat sink or heat spreader), whereas for TIM2 applications, both heat transfer surfaces are ideally metal. Regardless, the most appropriate measurement is that which not only takes into account the heat transfer across the bulk TIM structure, but also the thermal contact resistances associated with the heat transfer into and out of the TIM across the TIM/heat transfer surface interfaces.

Perhaps the most common instruments for TIM characterisation are those which follow ASTM D5470 'Standard Test Method for Thermal Transmission Properties of Thermally Conductive Electrical Insulation Materials' [45]. This method utilises opposing metre bars of known thermal conductivity, one heated and one cooled, to sandwich the TIM, thus emulating the mating heat transfer surfaces in practical applications. As described recently in Refs. [46–49], the metre bars are constructed in such a way that one- dimensional heat conduction is ensured along their length. In this way, imbedded thermal probes (thermocouples, RTDs, thermistors) can measure the associated temperature gradient as well as extrapolate the hot and cold side heat transfer surface temperatures. The product of the temperature gradient and the metre bar thermal conductivity gives the heat flux across the thermal joint containing the TIM, and together with the measured difference in the hot and cold surface temperatures, is sufficient to calculate its net thermal resistance. The main benefits of the ASTM D5470 method are: the measured thermal resistance includes the contribution of the thermal contact resistances between the TIM and the heat transfer surfaces, the applied load can easily be varied and measured, the operating temperature can be varied, the surface roughness can be controlled and the bond line thickness can easily be measured facilitating the estimation of the effective thermal conductivity. However, high-performance TIMs will result in low thermal resistance across the joint and special care must be taken to ensure adequate accuracy of the temperature measurements whilst minimising excessive heat transfer from the metre bars to the surroundings [46,47].

A related technique that has recently been developed is that whereby IR microscopy is used opposed to imbedded temperature probes [50–53] in an ASTM D5470-type assembly. This technique uses high-resolution IR thermography to measure the thermal gradients in a focussed region of the thermal joint in order to address resolution limits offered by the standard ASTM D470 instruments. Smith et al. [50] demonstrated the technique and were able to measure thermal resistances of solder joints down to 0.01 ±0.001 cm^2 KW^{-1} which is impressive. A further benefit is that this method can measure the thermal gradients across various layers in a TIM stack assembly, thus facilitating the measurement of the contribution of each layer, including those of semiconductor dies and interfaces, to the overall thermal resistance of the TIM [51].

The principle drawback of the ASTM-type methods is that they do not necessarily mimic the thermal-mechanical condition of real IC packages. Thermal test vehicles (TTV) facilitate the measurement of the TIM thermal resistance in situ and thus better represent the performance in practical application [4]. Lee et al. [54], for example, illustrated this by using a TTV adhering to the JESD51-2 standard procedure setup, where a Flip Chip Ball Grid Array package was used as the device under test. Taylor and Garimella [55] developed a novel TTV with embedded capacitance sensors aimed to measure the bond line thickness and detect voids in thin layers of dielectric TIMs, such as thermal greases, offering a new method for quantifying the degradation in the quality of TIMs over long-term usage. Na et al. [56] used a transient technique whereby a semiconductor power chip was used as both the heat source and the temperature sensor. Using a Mentor Graphics T3Ster1.1C, a heat pulse is initiated at the die and the test chip temperature monitored over a prescribed time interval. The temperature-time history is then analysed using structure functions, which decompose the signal into constituent components along the thermal pathway facilitating the estimation of the thermal resistance across each thermal impedance zone, including the TIM.

Another popular transient technique used to evaluate TIM thermal characteristics is the flash method [57]. This instrument typically uses an IR detector to measure the temperature rise curve of a sample that has been subject to an energy burst on the opposing side from a laser or xenon flash lamp, yielding the thermal diffusivity of the test sample. In order to determine the thermal conductivity, the specific heat and density must be measured separately. Although typically suited for free-standing thin, solid, and homogeneous test samples, it has been adapted for sandwich-type TIM assemblies to simulate realistic thermal-mechanical loading conditions of IC packages [58].

In the context of TIM thermal characterisation, the instruments and methods outlined above are particularly well suited because they include the practicality associated with the thermal contact resistance between the TIM and the outer heat transfer surfaces. Somewhat less ideal are those instruments and methods which only measure the thermal resistance and/or conductivity of TIM assemblies. That is not to say that these approaches are not useful in the earlier stages of TIM development, especially for diagnosing localised thermal transport phenomena which is not afforded by bulk resistance measurements.

5. Different types of thermal interface materials

Structured carbon TIMs

The extremely high thermal conductivity of pure carbon material makes it an obvious candidate for high-performance TIMs. One approach is to use carbon-based fillers, such as diamond, carbon nanotubes (CNTs), graphite and graphene as filler material in a polymer matrix to form composite pastes and epoxies of higher thermal conductivity than can be afforded by using conventional filler material, such as metals and ceramics which have significantly lower thermal conductivity. However, with the advent of new material fabrication techniques, in particular that of producing novel nano-materials, a fairly new category of structured carbon TIMs has appeared over the past decade or so.

The structured carbon TIMs receiving most of the attention in the literature are those fabricated from carbon nanotubes (CNTs). The proportionately large amount of research being conducted on CNT-TIMs is due to their very high intrinsic thermal conductivity and that they are mechanically compliant. Theoretically, a single-walled nanotube (SWNT) has been reported to have a thermal conductivity as high as 37 000 $Wm^{-1} K^{-1}$ [59] whereas multi-walled nanotubes (MWNTs) have been reported to have up to 3000 $Wm^{-1} K^{-1}$ at room temperature [60,61]. From a mechanical perspective, CNTs have a low transverse elastic modulus and are able to adapt to and conform to considerable external loads without any permanent atomic alterations [62]. Thus, they can potentially absorb stresses incurred by CTE mismatch between semiconductor dies and metals in a device package [63]. It is now established that vertically aligned carbon nanotubes (VACNTs) are ideal as they offer the maximum thermal conductivity and mechanical compliance [63,64]. Importantly, CNTs can be grown in arrays of relatively high density [56]. Dense forests of VACNTs are desirable since the higher number of CNTs thermally communicating heat between mating surfaces, the lower the bulk thermal resistance. Other benefits of CNTs are their good chemical stability and low CTE [54].

The earliest embodiments of CNT-TIMs were fabricated directly on Si wafers [65,66]. Xu and Fisher [65] demonstrated that CNTs were a viable TIM technology by fabricating free-standing forests on Si and subsequently measuring the thermal resistance in an ASTM D5470 TIM tester. A minimum resistance of ~0.2 $cm^2\ KW^{-1}$ was measured at a reasonable load of 0.445 MPa. The magnitude was remarkably consistent among different researchers [66–72], though it is noted that this is as good as typical commercially available thermal greases and significantly larger than lead-free solders [73]. The limited performance of the CNT-TIMs, compared with what might be expected considering their exceptionally high intrinsic thermal conductivity, is largely due to the high thermal contact resistances between the CNTs and the substrate [73– 75]. This was recognised early in the technology demonstrator stage of CNT-TIMs, where CNT array–substrate interfacial thermal resistance was determined to be ~0.1 $cm^2\ KW^{-1}$ [66], which is compounded by the fact that there will be two interfaces in a viable CNT-TIM. In short, because there is no chemical bonding or special association between the CNTs and the substrate at the atomic or molecular scale, this thermal boundary resistance becomes the limiting thermal resistance [52,66,76,77], though other aspects including but not limited to the quality of the CNTs [64], the volume density [56] and the degree of tangling [59,62] must also be considered as they all can influence the bulk thermal conductivity.

Another key practical issue that must be addressed when considering CNT structures as TIMs is that they are fabricated in a very harsh environment. Specifically, high temperatures (>700°C), long heating times (>5 min) and exposure to corrosive substances (e.g. H_2, NH_3 and plasma) negate the possibility of growing the CNTs directly on semiconductor electronic devices [64]. Thus, a CNT transfer process technology must be engineered for moderate temperature and practical implementation in electronic packages. One approach is to use a sacrificial growth substrate using conventional fabrication technology, such as chemical vapour deposition (CVD), and later transfer to the processed die. Another approach is to synthesise CNTs on high thermal conductivity substrates, like Cu, by using an intermediate buffer layer. Of course, good adhesion and low interface contact resistance between the individual CNTs and the transferring substrates in the resulting 'synthesised sandwich' [77] structure is a key requirement, in the sense that transferability and contact resistance must be considered in together.

The above considerations are driving the current CNT-TIM research, where the state of the art is being progressed by considering technologies and approaches that can produce low cost, high quality and reliable transfer process of well-aligned high thermal conductivity VACNT arrays with low contact resistance between the CNTs and the transfer substrates.

Lee et al. [54] recently synthesised VACNTs on Cu substrates and considered strengthening of the arrays by impregnating them with Cu or epoxy. The tips were subsequently exposed and the assembly tested in a thermal test vehicle-type JESD51-2 TIM tester. A limited performance of 0.277 $cm^2\ KW^{-1}$ was measured for the epoxy-sealed CNT-TIM at an assembly pressure of 1.1 MPa, with the Cu-sealed CNT-TIM about twofold higher at the same assembly pressure. Na et al. [56] collated previous data and determined a general trade-off between mass density of a CNT forest and the height of the CNTs. Focussing on fabricating denser and taller CNTs on Cu foils that could potentially conform to surface roughness of practical heat transfer surfaces, they optimised the catalyst/under layers and CVD conditions to realise VACNTs of ~50 μm in height with mass density of ~0.3 $g\ cm^{-3}$. The assemblies were sandwiched between Cu and Al blocks with surface roughness in the region of 20–30 μm and tested using the Mentor Graphics T3Ster1.1C under an assembly pressure of 0.34 MPa. The results confirmed that increasing the mass density of CNTs decreased the overall thermal resistance, achieving as low as 0.24 $cm^2\ KW^{-1}$, and noted that this is comparable to a thick (100 μm) indium foil TIM. Yao et al. [63] evaporated Ti, Ni and Au onto the VACNT array, grown on a sacrificial Si substrate, as well on Si and Cu heat transfer surfaces. Thin (25 μm) indium foils were attached to all four metalised surfaces and the stack assembly heated at moderate temperature (200°C) to bond them together, thus illustrating successful transfer from a growth substrate to a device. A thermal resistance as low as 0.034 $cm^2\ KW^{-1}$ was achieved with CNTs synthesised in the commercial AXITRON Black Magic CVD machine, which was significantly lower than the lab-grown version highlighting the importance of CNT quality. Ganguli et al. [73] grew VACNT arrays on thin graphite substrates. Measurements revealed that the all carbon atomic configuration formed catalyst-free covalent bonding at the CNT-graphene junction resulting in a measurable reduction in the associated thermal boundary resistance to ~0.06 $cm^2\ KW^{-1}$, though there was a high fraction of CNTs that were not ideally bonded so there is considerable room for improvement. Bar-Cohen et al. [78] discussed a novel transferable

CNT-TIM whereby VACNTs were synthesised on both sides of a graphene foil carrier. The CNT tips were metalised in order to solder them to the mating heat transfer surfaces. Thermal resistances as low as 0.02 cm^2 KW^{-1} were measured for an assembly of 100 µm thickness, representing an order of magnitude or more improvement over conventional TIMs and likely the lowest thermal resistance for transferable CNT-TIM technologies to date. Importantly, this CNT-TIM showed stability when subject to thermal cycling and high-temperature baking, thus demonstrating potential for long-term reliability in application.

Thaphouse et al. [79] investigated a potentially scalable and low cost approach by spray coating VACNT forests with nanoscale polymer coatings. The polymer coatings on the tips of the CNTs were bonded to adjacent substrates by dissolving them in solution at room temperature and then pressing them at moderate pressure (138 kPa) and allowing the polymer to dry. A transfer technology was demonstrated by growing VACNT forests on both sides of a 10 µm Al foil achieving a thermal resistance of 0.09 cm^2 KW^{-1}. McNamera et al. [53] developed a transfer process by growing VACNTs on a Si substrate, pressing and anchoring the free ends onto a thermal contact adhesive (TCA) coated Si substrate, representing a die, and then peeling off the growth substrate. A second TCA-coated Cu surface was then pressed onto the free ends of the array and cured to anchor these ends of the CNTs. A similar approach was used with indium opposed to TCA. IR microscopy and a bespoke test fixture was used to measure thermal resistances as low as 0.04 cm^2 KW^{-1} for the TCA assembly and 0.09 cm^2 KW^{-1} for that of indium. Although performing well, it was thought that the full arrays were not participating in the thermal transport due to poor CNT infiltration into the bonding substrates. Importantly, thermal cycling and thermal aging tests were performed showing limited degradation of the TCA assembly, though a large drop in performance for the indium assembly.

As depicted in Figure 5, Barako et al. [52] transferred VACNT arrays to a metalised target substrate using a reactive metal bonding layer as well as indium solder to anchor the CNTs and subsequently peel them from the growth substrate. Comparative IR microscopy was used to evaluate the thermal resistances of the bonding interface in situ both before and after bonding. The tip-interface resistance was measured to be ~0.3 cm^2 KW^{-1}, which was an order of magnitude lower than the un-bonded joints and was independent of pressure indicating that high-quality metallic bonds were formed.

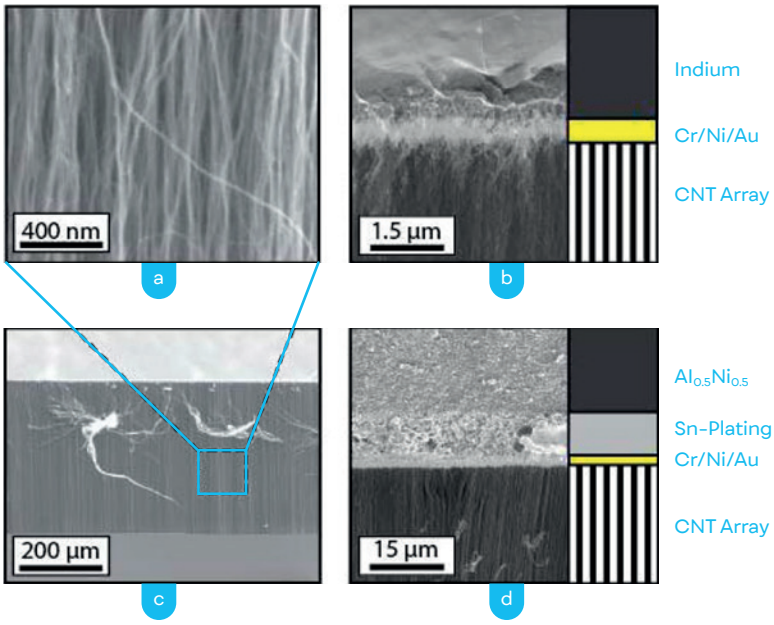

Figure 5. (a) SEM image of vertically aligned CNTs highlighting the morphology and (b) corresponding CNT array on a silicon growth substrate. (c) higher magnification image showing the interface of a CNT array bonded using indium foil and (d) reactive metal. Adapted from Barako et al. [52]. Copyright 2016, IEEE. Reprinted with permission.

Similarly, Peacock et al. [62] transferred VACNTs from the growth substrate to Cu heat transfer surfaces and bonded them via solder on each side. Using an ASTM D5740 TIM tester, the thermal resistance of 0.458 $cm^2\ KW^{-1}$ was reported at 0.14 MPa, with a small reduction when the applied pressure was approximately doubled indicating some incomplete contact of the CNTs. The limited performance of the CNT-TIM was discussed in terms of the various contact resistances in the stack, including that between the TIM assembly and the heat transfer surfaces. Qiu et al. [80] also considered the interface resistance between a CNT-TIM and the heat transfer surface by developing a shear pressing technique which ostensibly bent the top portion of the CNTs so that they are parallel to the mating substrates. The idea is that this forms a line-contact between the horizontally aligned CNTs and the mating surface, opposed to the near point con- tact associated with VACNTs. The 3-ω technique was used to evaluate the different thermal resistances in the stack assembly showing a low thermal boundary resistance between the horizontal CNT tips and mating substrate of 0.035 $cm^2\ KW^{-1}$.

Albeit to a much lesser extent compared to VACNTs, structured carbon TIMs have been proposed using other carbon compounds. 3D graphene monoliths have been considered due to the high intrinsic thermal conductivity of graphene and high flexibility under compression [81–83]. However, limited performance is observed owing to the high porosity required to make them mechanically compliant. Very recently, Lv et al. [84] fabricated super-elastic graphene/CNT aerogels by a hydrothermal method with subsequent freeze-drying. The 3D framework, shown in Figure 6, was constructed from graphene sheets entangled with CNTs, which bonded the graphene sheets together in order to stop them from sliding under compressive loading thus giving the structure super-elastic properties. Gr/CNT-TIM samples were tested in an ASTM D5470 TIM tester with an effective thermal resistance in the range of 0.136–0.195 $cm^2\ KW^{-1}$ at moderate pressures. The performance was comparable to the best performing Gr-TIM reported in the literature, that being vertically aligned functionalised multilayer graphene [85].

Vertically aligned graphite has also been considered as a high-performance TIM [78]. Here, graphite nano-platelets were compressed into flexible sheets and imbedded in solder with the high conductivity plane aligned perpendicular to the mating heat transfer surfaces i.e. in the primary heat transfer direction. An impressive 0.01 $cm^2\ KW^{-1}$ was reported at a bonding temperature of 230°C and assembly pressure of ~0.2 MPa. Sharma et al. [86] also investigated graphite-solder TIM. Here, the composite sheets were fabricated to form graphite networks with a reflowed process to form the solder network from fluxless solder powder. Tested in an ASTM D5470 device, thermal resistances in the region of 0.05 $cm^2\ KW^{-1}$ were achieved at pressures below 0.1 MPa, with the interface resistances with the heat transfer surfaces being posed as dominant. Nanostructured mats of graphene nanoplatelets and carbon nanotubes and nanofibers were synthesised by Warzoha et al. [87]. The graphene was introduced as a comparatively high surface area structure within the composite to mitigate phonon scattering, an endemic problem with nanostructured networks. Excellent performance, with thermal resistances as low as 0.01 $cm^2\ KW^{-1}$ at a load of 0.56 MPa, were confirmed by measurement in an ASTM D5470 TIM tester.

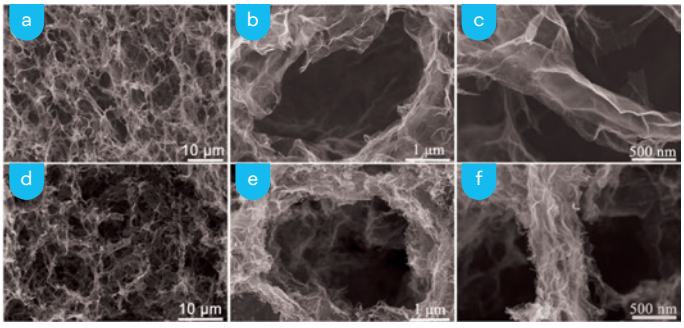

Figure 6. SEM images of 3D porous structure of (a, e, c) neat graphene aerogel and (d, e, f) gr/CNT-2 aerogel with similar initial density. Microscopic cellar wall architecture consisting of partially (b) overlapping graphene sheets and (c) wrapping graphene sheets for neat graphene aerogel, and entangled CNTs covering overlapping graphene sheets and (f) wrapping graphene sheets or gr/CNT-2 aerogel. Adapted from lv et al. [84]. Copyright 2016, Elsevier. Reprinted with permission.

Metals: solders and low melting temperature alloy TIMs

The application of solder and low melting temperature alloys are well known in the thermal interface materials community for more demanding application areas which require effective thermal interface materials with high thermal conductivity and thermal resistance as low as 0.05 $cm^2\ KW^{-1}$. So far the best value in terms of thermal resistance was reported for liquid mercury droplets on a gold plated Si die, which showed a resistance as low as 0.00253 $cm^2\ KW^{-1}$ [88]. However, Mercury is impractical as a TIM due to obvious health and safety issues. Martin and Kessel reported an excellent thermal resistance of 0.02 $cm^2\ KW^{-1}$ with an effective thermal conductivity of 31 $Wm^{-1}\ K^{-1}$ for an undisclosed liquid metal [89], whereas Hill and Strader showed a low thermal resistance of 0.017 $cm^2\ KW^{-1}$ for Cu foil coated with indium–bismuth–tin alloys of thickness 130 µm (developed by coating alloys on both sides of a 70 µm nickel plated Cu disk) at 68.9 kPa [90].

In order to investigate the thermal properties of these low melting point alloy, Roy et al. investigated the thermal performance of the Ga, 75.5% Ga 24.5% In and 51% In 32.5% Bi 16.5% Sn alloys by measuring the thermal resistance according to the ASTM D5470 standard [91]. A thermal interfacial resistance of as low as 0.005 $cm^2\ KW^{-1}$ was achieved for pure InBiSn solder or Field's alloy which has a melting point of ~60°C when measured between tungsten coated Cu disks, whereas with bare Cu disks the average value was 0.03 $cm^2\ KW^{-1}$. It was observed that the measurements of the solder-based TIM were largely dependent on the surface roughness and planarity of interface of the metre bars. Furthermore, the quality of the wetted surface (using solder TIM) plays a major role in defining the thermal resistance of the interface. Ageing study on the Field's alloy by heating the TIM to 100°C for 800 h showed that there was only 15% degradation in the thermal resistance from 0.048 to 0.055 $cm^2\ KW^{-1}$ whereas for an indium deficient (as compared to 51% In) alloy (26% In 57% Bi 7% Sn) the resistance increased almost 51% from the initial value of 0.098 $cm^2\ KW^{-1}$ [92]. This is due to the fast interfacial reaction with the Cu disk, which resulted in an intermetallic compound to be formed at the expense of indium and tin and ultimately resulted in the formation of brittle Bi phase in the TIM layer. This brittle phase initiated cracks and expanded with the ageing and ultimately increased the thermal resistance as can be seen in Figure 7.

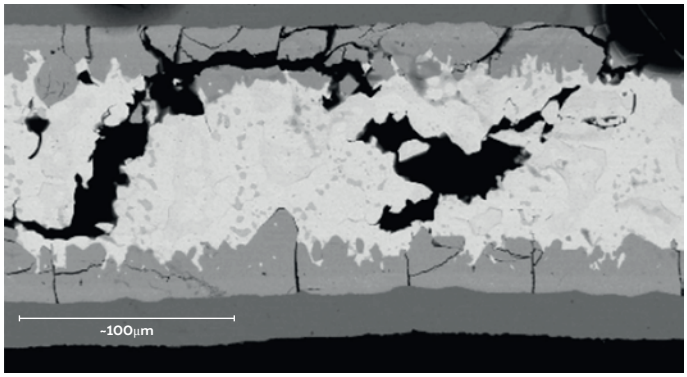

Figure 7. SEM image of failed cu/17sn51in32bi/Cu sandwiched sample after aging at 150 C for 400 h. Adapted from Yang et al. [92]. Copyright 2016, Springer. Reprinted with permission.

Accelerated aging tests performed at an elevated temperature of 130°C on Ga–In material showed an increase in resistance from 0.02 to over 0.05 $cm^2\ KW^{-1}$ between 1000 and 1500 h, but did not change thereafter for up to 3000 h. However, for Ga and Field's alloy no major change was measured though an interfacial crack was observed after heating at 150°C for 400 h [93]. Similarly, thermal cycling tests showed that for the Ga–In alloy, the resistance increased within the first 300 cycles and then remained relatively constant up to 1500 cycles. In case of Ga and Field's alloy no notable change was observed.

One significant drawback of these pure materials and alloys is that they can be easily deformed due to low yield strength and thus have a risk of flowing out during the attach process, which might result in short circuits in application. Furthermore, the large thermal expansion coefficient of the TIM as compared to Si chip and heatsink can result in thermal fatigue and segregation of the TIM. As noted by Bar-Cohen et al., the low mechanical compliance and risk of high stress failure for thin (25 μm–50 μm) bond line thicknesses necessitates that a minimum thickness of around 200 μm be used [78]. Thus, the high thermal conductivity is offset significantly by the requirement of a relatively thick TIM in application. To address this, a high thermal conductivity phase (e.g. diamond, Cu, Ag, etc.) uniformly distributed in a high mechanically compliance phase (In, Sn, etc.) similar to the polymer composite-based TIM has been proposed by Liu et al. [94]. In order to study the impact of the interfacial layers in the Cu–In composite, Cu particles were coated with three different types of interfacial layers namely, 50 nm Au, 1 nm Al2O3 and 1 nm Al2O3 followed by 20 nm Au prior to mixing with In. In terms of effective thermal conductivity, samples without any interfacial layer (40% Cu–60% In) were recorded to have conductivity values which dropped rapidly by 23% after 96 h in the accelerated ageing experiments done at 125°C. For the sample with 1 nm Al2O3 coating the effective conductivity of the compo- site even reduced further and retain only approximately 75% of In but the deterioration due to ageing was minimal (3.7%). On the other hand, in the case of the 50 nm Au-coated sample, which enhances the interfacial wetting via reaction with liquid In to form $AuIn_2$ and reduced voids, showed enhanced thermal conductivity as compared to In. However, ageing resulted in a 10% reduction in conductivity after 100 h. The 1 nm Al2O3/20 Au-coated sample showed the highest thermal conductivity of approximately 125 $Wm^{-1} K^{-1}$, an improvement of 52% over In and only 3% reduction after 96 h of ageing. A thermal resistance of 0.021 $cm^2 KW^{-1}$ was reported with a shear yield strength of 2.7 MPa, which is about twice that of In and still remain bonded.

In a similar study by Sharma et al. [95], a Cu–In composite was fabricated using liquid phase sintering (LPS), quenching and subsequent accumulative roll bonding and, with different vol.-% Cu, resulted in a maximum effective conductivity of 151 $Wm^{-1} K^{-1}$ for 40% of Cu in an In matrix (Figure 8). The conductivity was estimated using Wiedmann–Franz Law from the measured electrical conductivity of the samples. Similarly, 42% Sn 58%Bi solder paste had been tested as a TIM between Cu disks using the laser flash technique, where the solder was melted at 180°C [96]. A thermal resistance of as low as 0.05 $cm^2 KW^{-1}$ was reported with a calculated thermal interfacial resistance of 0.0057 $cm^2 KW^{-1}$ between the Sn–Bi solder alloy and the Cu disk. It was also reported that the thermal resistance generally decreased marginally after thermal cycling tests, showing good reliability for the Sn–Bi-based TIM, though the alloy was found to suffer from poor wettability on Cu disks as observed in scanning acoustic microscopy analysis.

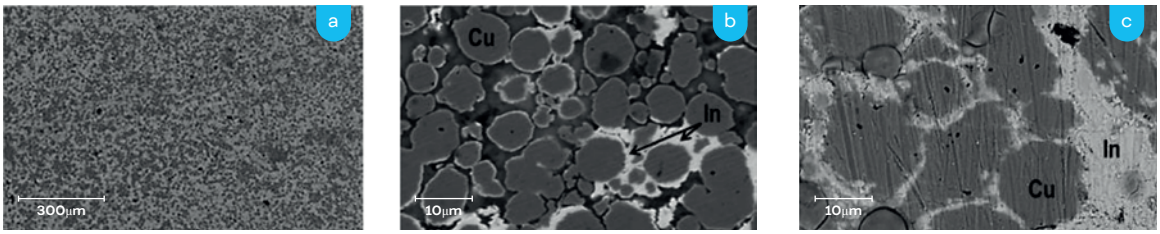

Figure 8. SEM micrographs of as-sintered samples produced after LPS at 160°C for (a) 30 s (low magnification), (b) 30 s (high magnification) and (c) 60 s (high magnification). Images were acquired using BSE. Dark regions-Cu. Bright regions-In. Black regionspores. Adapted from Sharma et al. [95]. Copyright 2016, IEEE. Reprinted with permission.

In order to improve the thermal performance, Luo et al. proposed boron nitride (BN) nanofiber–In composite as a thermal interface material, where the thermal conductivity and resistance were calculated from the diffusivity values measured using the Xenon flash technique [97]. Due to the anisotropic nature of the BN nanofibers, an in-plane thermal conductivity of 60 $Wm^{-1} K^{-1}$ and cross-plane thermal conductivity of 20 $Wm^{-1} K^{-1}$ was measured, whereas a low thermal resistance of 0.02 $cm^2 KW^{-1}$ was achieved for 31.3% BN and 68.7% In composite. As mentioned, CTE mismatch is one of the major issues in the application of low melting point metals and alloys. To improve the CTE, Raj et al. co-deposited SiC and graphite using a commercial tin bath [98]. A 30 and 70% volume loading was achieved for the SiC and graphite particles in the composites, which was projected to achieve a CTE of 5–10 ppm $°C^{-1}$, which is in the range of semiconductor material. The authors also estimated a thermal conductivity enhancement of 50–100% though no value was reported.

Metal foil with microtextured surface have been proposed by Kempers et al. where the authors modelled and fabricated 36 and 28 µm thick Ag foils with cones approximately 0.95 mm tall and 1 mm base on a 2 mm pitch [99]. The concept was aimed to target the interfacial contact resistance and associated intimate contact area by using a compliant metal and then plastically deforming the small structures when the two opposing faces were compressed. The concept was demonstrated to have an effective thermal conductivity of between 4 and 7 $Wm^{-1} K^{-1}$ and associated thermal resistance as low as 0.6 $cm^2 KW^{-1}$ at a pressure of 1.5 MPa. The same TIM concept was later deployed using tin which reduced the thermal resistance below 0.1 cm2 KW^{-1} at the same assembly pressure [100].

There is a growing interest in metal nanotextured surfaces as next-generation TIMs owing to their high intrinsic thermal conductivity and mechanical compliance. Razeeb and Roy proposed a Ni nanowire–Alumina composite where the nanowires are high aspect ratio structures such that an individual wire can make thermal contact across the two heat transfer surfaces whilst conforming to micron scale unevenness of the mating surfaces [101]. An intrinsic thermal conductivity of 70.7 $Wm^{-1} K^{-1}$ was reported for 308 nm diameter Ni nanowires with an average length of 62 ± 2 µm. These metallic nanowires can be also embedded inside flexible and conformal polymer matrix which, as described in the section 'Filler-type TIMs: pastes, epoxies, adhesives, etc.', can be an effective thermal interface material. Feng et al. as shown in Figure 9 proposed double layered Sn nanowires as TIMs [102]. In their work, nanowires were grown on both sides of the metal foil, which resulted in free-standing double-sided nanowire arrays with a measured thermal resistance of 0.2 $cm^2 KW^{-1}$ under a pressure of 1 MPa. Barako et al. fabricated dense arrays of Cu nanowires directly onto substrates via templated electrodeposition [103]. The anisotropic structures achieved a maximum axial thermal conductivity of 70 $Wm^{-1} K^{-1}$ with an associated lateral conductivity in the region of 2 $Wm^{-1} K^{-1}$.
In a recent review of TIMs for DoD applications, Bar-Cohen et al. report the development of a compliant nano-TIM comprised of Cu nano-springs fabricated by glancing angle deposition.
The nanostructured layer was made transferable by plating with Ni on each side and subsequently soldering to the heat transfer surfaces. The nano-spring TIM was more than 100× more compliant than solder bonding and achieved a thermal resistance less than 0.01 $cm^2 KW^{-1}$ [78].

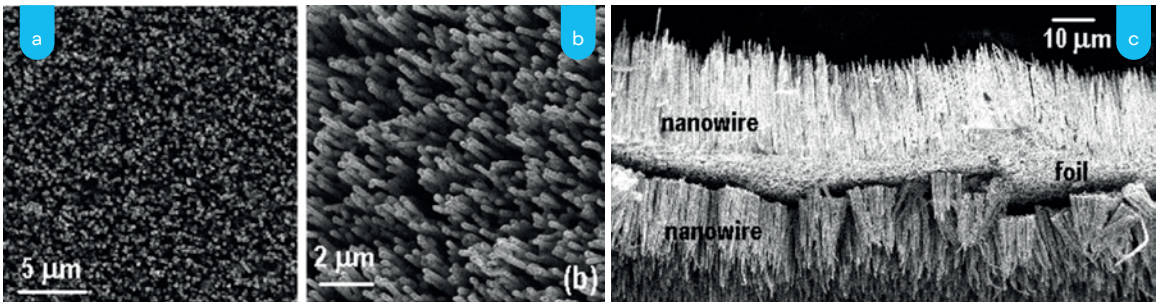

Figure 9. SEM images of double-sided tin NW arrays (a) top view, (b) side view and (c) cross-sectional view. Adapted from Feng et al. [102]. Copyright 2016, American institute of physics. Reprinted with permission.

Filler-type TIMs: pastes, epoxies, adhesives, etc.

Due to their low cost, ease of application and reasonable performance, thermal pastes/greases, and to a lesser extent adhesives and epoxies, have become the 'go-to' solution to mitigating excessive contact resistance in electronic packages and devices [4]. The urgent necessity of novel and reliable high-performance TIMs from the semiconductor device industry has drawn the attention of researchers during the last decade to improve upon these already available 'tried-and-true' commercial offerings [5]. To this end, novel filler- type TIM technologies based on carbon e.g. CNTs, graphite, diamond and amorphous carbon, as well as other high conductivity filler particles are being studied among academic institutions and industry.

The current research in the broad area of filler-type 'spreadable' TIMs can be roughly divided into films, pastes and epoxies. In each case the general idea remains similar; a high conductivity filler material, be it CNTs, graphite/graphene or other nano or micro particles, are added to a mechanically compliant and much poorer thermal conductivity polymer, phase change material (PCM) or epoxy matrix. The compromise to be struck is that sufficient filler material must be introduced to achieve a reasonable bulk thermal conductivity by reaching the percolation threshold, without making the compound so stiff that it cannot form a thin bond line or displace the air trapped in the grooves and imperfections of the mating surfaces.

Due to their very high intrinsic thermal conductivity, CNTs have been considered as an alternative filler in spreadable TIMs. These nanocomposites use the CNTs as filler materials to tune the thermo-mechanical and sometime electrical properties of the TIM. The performance of these nanocomposites depends strongly on the type of CNTs, matrix materials, the loading percentages and the TIM-surface characteristics. However, the introduction of CNTs and other nanoparticles into a polymer matrix is not a straightforward process, and the mixing and dispersion of the materials has a significant impact on the overall thermal performance.

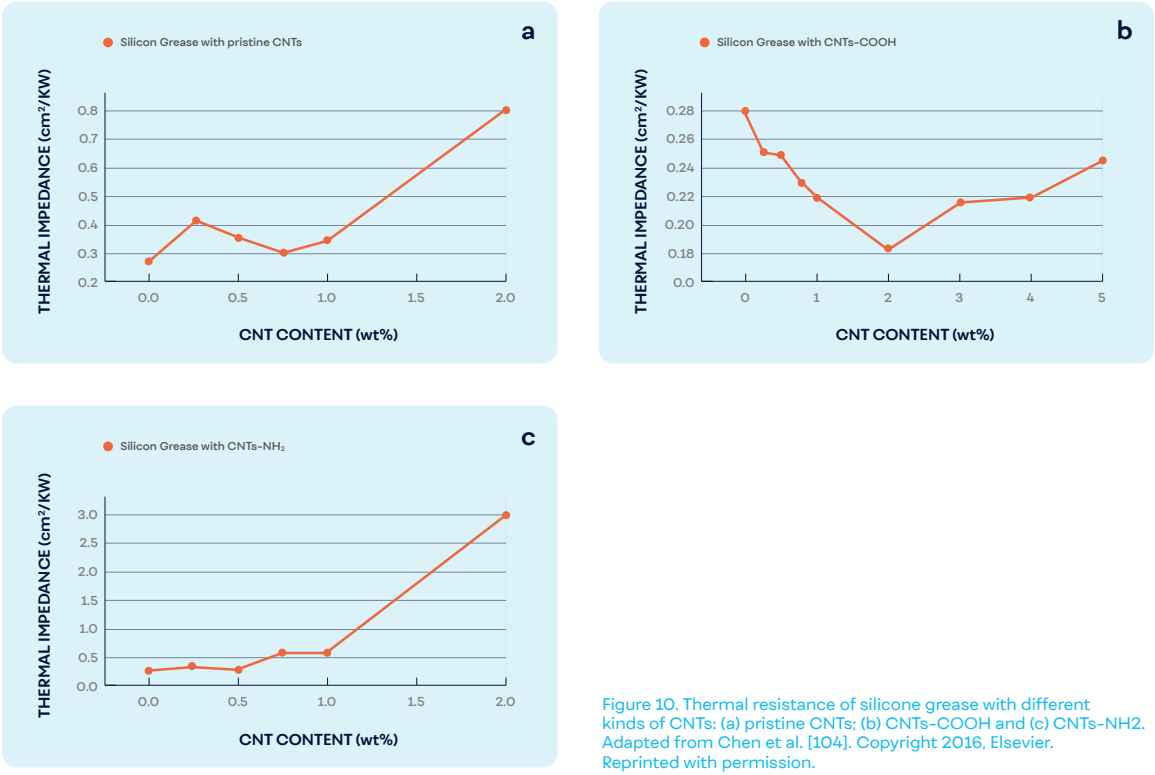

Figure 10. Thermal resistance of silicone grease with different kinds of CNTs: (a) pristine CNTs; (b) CNTs-COOH and (c) CNTs-NH2. Adapted from Chen et al. [104]. Copyright 2016, Elsevier. Reprinted with permission.

This was identified by Chen et al. [104] who showed that the addition of unmodified CNTs into a commercial silicone grease TIM could in fact degrade performance of the composite as a function of particle loading. However, modifying the CNTs with carboxylated showed a measurable decrease in the thermal resistance from 0.28 to 0.18 cm^2 KW^{-1} for a 2wt-% loading, though further increase in particle loading once again increased the thermal resistance, this is shown in Figure 10.
This improvement of modified over unmodified CNTs was attributed to improved dispersion of the CNTs in the polymer matrix. In each case of modified and unmodified filler material, above ~2 wt-% tends to increase the thermal resistance of the composite, and this was also observed by Kiran et al. [105]. In this work, a commercial silicone grease TIM was loaded with unmodified multiwall CNTs and a relative increase in the effective thermal conductivity of ~40% was achieved with particle loading between 1 and 2%. As with other studies, further increases in loading deteriorated performance.

This increase is explored in more detail by Zhang et al. [106], using multi-walled CNTs of between 5–10 µm length, together with carboxylic acid groups and nano-copper particles incorporated into an epoxy resin to form hybrid composites. Testing particle loadings up to 15wt-% of CNTs and 70wt-% of nano-copper, they found that the bulk thermal conductivity was somewhat insensitive to particle loading. However, they did find that the contact resistance of the composite increased as a function of particle loading, and this influenced the overall thermal resistance above 10% loading.
This relationship of contact and bulk resistance is shown in Figure 11.

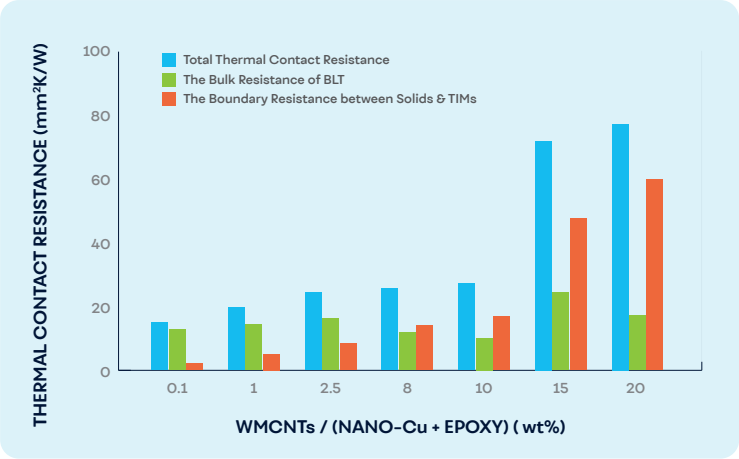

Figure 11. RBLT and RB1 + RB2 of the nano-copper/epoxy resin composites filled with different MWCNT proportions in weight at 1 MPa pressure loading (the BLT is about 5 µm). Adapted from Zhang et al. [106]. Copyright 2016, Elsevier. Reprinted with permission.

In the cases discussed above, the filler materials are non the nanoscale and as such introduce some technical challenges not necessarily associated with microscale particles. These include, though are not limited to, producing uniform dispersion of the nanoparticles within the matrix material [107], large filling percentage for percolation [108] and the introduction of significant contact or boundary resistances (between particles), also known as Kapitza resistances [109]. Furthermore, the surface condition of the nanoparticles can play an important role. For example, Yujun et al. [110] showed that surface modifications on CNTs could strongly influence the effective thermal resistance of a composite thermal grease. By developing various CNT-TIM grease nanocomposites formulations, with various CNT lengths, some modified with strong acids or bases, it was shown that a significant improvement in thermal resistance could be achieved over the base silicone TIM. Substantially, the data showed that 2wt-% loading of short length (2–3 µm) modified MWCNTs can reduce the thermal resistance from 2.89 to 1.37 cm^2 KW^{-1}, a reduction of 52.6%. The same was not observed for the unmodified CNTs. Along the same theme of surface modifications, Ahn et al. [111] coated copper nanowires with titanium oxide to enhance the mechanical and thermal properties in the polymer matrix. The TiO_2-coated copper nanowire/epoxy composites exhibited thermal conductivities ranging from 0.2 to 1.12 Wm^{-1} K^{-1}, values that are higher than those of raw copper nanowire/ epoxy composites at the same weight fraction.

Of course the type of filler material is a crucial factor with regard to the effective bulk thermal conductivity of the composite material for filler-type TIMs. Although CNTs have been shown to have very high intrinsic thermal conductivities and offer a potential for high thermal conductivity composite TIMs, they are still an expensive material. As such, researchers have tried implementing lower cost carbon substitutes like graphite and graphene as fillers. Kim et al. [112,113] used a combination of graphene and CNTs to produce a spreadable nanocomposite TIM specifically engineered for LED cooling applications. It was determined that the thermal conductivities of CNT-Gr grease enhanced up to 16% and 6% at 0.75 wt-% of the nanoparticles, respectively, compared with the baseline thermal grease. It was shown that the maximum loading concentrations of nanoparticles was 0.75 wt-%, and a higher percentage impacted negatively on the thermal resistance due to solidification of the composite paste such that the TIM could no displace the air voids between the heat transfer surfaces. Raza et al. [114] developed an epoxy-based hybrid composite using boron nitride and vapour grown carbon nanofibers, with the primary motivation being that of producing a thermally conductive yet electrically insulating composite TIM. A maximum thermal conductivity of 1.74 $Wm^{-1} K^{-1}$ was obtained for a composite consisting of 1 wt-% MWCNT and 50 wt-% BN compared to 1.0 $Wm^{-1} K^{-1}$ for a composite having 50 wt-% BN particles only. This increase in the thermal conductivity was attributed to the formation of three-dimensional thermal transfer pathways between the BN and the MWCNTs. This work highlights the importance of the internal thermal networks formed within these filler-type spreadable TIMs. Using different filler material of different shapes and microstructures can be advantageous if they together form interlinkages that are better able to transfer the heat within and between the high conductivity filler phases. To this end, Nakajimi et al. [115] used a combination of hexagonal boron nitride (h-BN) platelets with plane diameter of 8 µm and thickness of 200 nm and diamond particles of 50 µm in a silicone matrix (Figure 12) to produce a composite TIM paste with a thermal conductivity of 6.1 $Wm^{-1} K^{-1}$. Interestingly, when only BN platelets were used a maximum thermal conductivity of 4.6 $Wm^{-1} K^{-1}$ was measured, which dropped to 2 $Wm^{-1} K^{-1}$ for the composite containing only diamond. The authors attribute the high performance of the BN-diamond paste to the increase in the number of thermally conductive networks resulting in an overall decrease in the thermal resistivity between the junctions of neighbouring diamond particles.

The use of high aspect ratio structures has one obvious benefit and that is their ability to achieve low percolation threshold in a nanocomposite compared to nanoparticles. This difference in aspect ratio is highlighted by Yu et al. [116] who used morphologically different materials that were elementally identical; these being silver nanowires (100 nm × 10–15 µm) and nanoparticles (~100 nm), both types surface modified with silane to produce an effective dispersion. They were able to show that the use of high aspect ratio structures allowed for a higher thermal conductivity for the nanowires (55.86 $Wm^{-1} K^{-1}$) compared to nanoparticles (8.44 $Wm^{-1} K^{-1}$) for the same percentage loading.

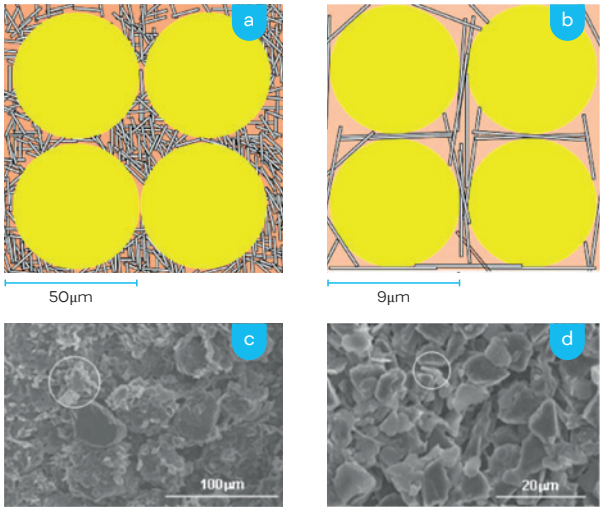

Figure 12. Schematic model of enhancement of thermal conductivity of mixed fillers consisting of h-BN filler and diamond having average sizes of 50 µm (a) and 9 µm (b). SEM micrographs of TIM with mixed fillers consisting of h-BN fillers and diamond having average sizes of 50 (c) and 9 µm (d). Aggregations measuring 20–50 µm and consisting of many h-BN platelets appear in (c) (one of them is indicated by the circle). Plane-to-plane bridging is apparent in (d) (one of them is indicated by the circle). Adapted from Nakajimi et al. [115]. Copyright 2016, the Japan Society of Applied Physics. Reprinted with permission.

The effect of the aspect ratio was also explored by Wang et al. who compared short copper nanowires (~100 nm × 20 µm) and long nanowires (~80 nm × 80 µm long) by placing them unmodified into a polyacrylate ester and cured to produce a composite film, the thermal conductivity as a function of volume loading is presented in Figure 13. The longer copper nanowires produced a significantly lower percolation threshold and higher thermal conductivity, by a factor of 6, over the shorter copper nanowires at equal percentage loading [117].

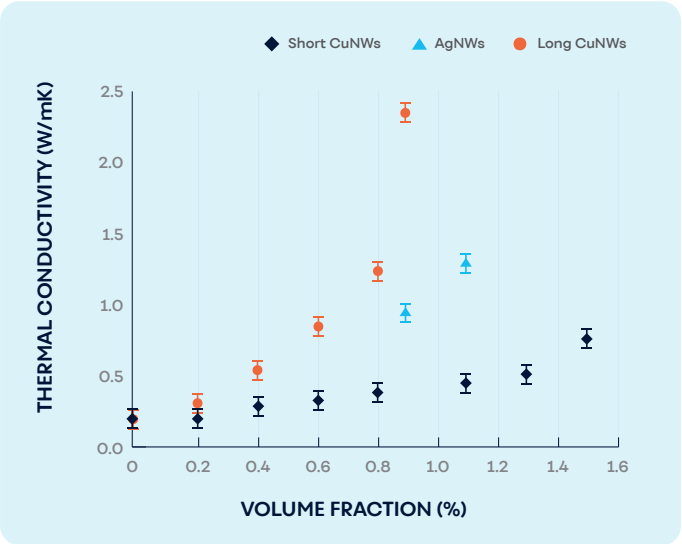

Figure 13. Experimental thermal conductivity of metal nanowire-polyacrylate composites with different volume fractions at 298 k. Adapted from Wang et al. [117]. Copyright 2016, American Chemical Society. Reprinted with permission.

Xu et al. [2] achieved a thermal resistance of 0.93 $cm^2\ KW^{-1}$ at an applied pressure of 1.0 MPa for electrodeposited silver nanowire-polycarbonate composite film, which was coated with 30 nm Au on the top. A thermal conductivity of 30.3 $Wm^{-1}\ K^{-1}$ was measured for the composite film where the nanowires showed a thermal conductivity of 334.6 $Wm^{-1}\ K^{-1}$. In a similar work [118], silver-silicone-based nanocomposite films fabricated using nanowire and flake structures was reported, where the nanowire-based composite showed a low percolation threshold as compared to flake-based composite. Later, Razeeb et al. reported Cu nanowire-polystyrene wax composite, where a thermal resistance of 0.09 ± 0.01 $cm^2\ KW^{-1}$ was achieved at a pressure of 100 kPa according to the modified ASTM D5470 standard, which is 50% lower compared to the commercial TIMs measured using the same system [119].

As the above implies, the filler particle size and shape has a number of important influences on the overall thermal resistance of the TIM. For example, large particles can produce a non-conforming surface, where the particle size is larger than the mating surface roughness, allowing air gaps to form. On the other hand, nanoparticles introduce a significant increase in the Kapitza resistance, which can impede heat flow through the composite material. Tang et al. showed that functionalisation reduces the Kapitza resistance between the filler material and the matrix [120]. Another method recently used to help obviate the effect of the Kapitza resistance is the use of high aspect ratio filler materials with equal percentage loading, where it is consistently found that the effective thermal conductivities of higher aspect ratio composites outperform those with lower ones [121,122].

6. Summary and outlook

Structured carbon-based materials are ideal for thermal interface application due to their high intrinsic thermal conductivity and mechanical compliance. Of these, carbon nanotubes, particularly vertically aligned CNT forests, have shown significant progress over the past decade. The challenges facing CNT-TIMs are associated with developing transfer processes that are amenable to semiconductor device fabrication and packaging constraints whilst ensuring high-quality CNTs and assemblies. In order to create CNT-TIM assemblies of as low as possible thermal resistance, research will continue to focus on methods that reduce the thermal contact resistance between individual CNTs and the mating substrates, including developing methods to increase substantially the number of CNTs that are correctly anchored to the substrate(s). Regardless, technology transition of CNT-TIMs seems eminent considering that some demonstrators have achieved overall thermal resistances in the region of ~0.02 $cm^2\ KW^{-1}$ and high-quality CNTs can now be fabricated in commercial machines, such as the AIX-TRON's Black Magic system. Other structured carbon-based TIMs, such as those fabricated with graphene and graphite, are still at an earlier technology development stage compared with CNTs. Even still, some very encouraging TIM technologies have been demonstrated. For carbon-based structured TIMs, reliability under long-term storage, thermal cycling and elevated temperature conditions is still mostly an open question that will require further accelerated stress testing to ensure adequate long-term operation in application.

For the metallic TIMs, re-workability and reliability of the TIMs are the two major issues that needed to be resolved. Reliability of the metal-based TIMs is a concern as pure metals and alloys oxidise during temperature cycle. Nanoscale coating with more stable material or nanocomposite formulation are fertile ground for future research. All the solder-based TIMs suffer from re-workability issues, where the cleaning of the TIM results in unnecessary financial burden. Research should be directed to solve this issue. Price is another major concern as compared to polymer-based TIMs. In and Ga are used in most of the low melting solder-based TIMs, which are comparatively expensive. Upscaling the technology for industrial production, while keeping the cost down using earth abundant elements (e.g. Sn, Ni, etc.) through micro-nanostructuring can be a way forward.

A great deal research has been performed in the area of composite filler thermal interface materials in recent years, with a strong focus on nanomaterial fillers. Researchers have made strides in producing composite materials, including nanocomposites, where the thermal conductivity of the material is significantly increased over the matrix alone. However, much of this research has not demonstrated the thermal resistance of said composites, which must of course include the interfacial contact resistance, thus not demonstrating the efficacy of the materials as potential TIMs. In general, loading a matrix with nano-materials increases its Young's modulus which can increase the interfacial contact resistance, and this can more than offset any gains in the bulk thermal conductivity. When a high-performance TIM is examined a low bondline thickness is preferred, and this accentuates the importance for low interfacial contact resistance as it becomes a higher percentage of the overall thermal resistance as the bond line thickness decreases. The future direction of filler-type spreadable TIM research must then carefully consider the mechanical behaviour, ensuring a thin bondline at allowable assembly pressures, whilst ensuring as low as possible interfacial contact resistance and as high as feasible bulk thermal conductivity. This is a highly nonlinear multiphysics problem involving mechanics, tribology and heat transfer and it would seem that modern simulation tools could be used to predict TIM behaviour and subsequently optimise their performance. The generation of an accurate model would be a significant step forward in producing the next-generation of filler-type TIMs and accelerate the advancement of the technology.

For raw performance, we anticipate a sharper focus on boundary resistance between the TIM and mating surfaces as material improvements alleviate the bulk conductivity vs. deformability trade-off. This is especially true for TIMs like carbon nanotube or metal nanowire forests where bondline thickness reduction is readily achievable with high thermal performance of the bulk due to increased forest density, but interfacial aspects are poorly understood. However, even conventional viscous TIMs appear to be close to a boundary resistance limit, which will need to be solved in part with more attention to wetting properties for example. Ultimately the industry appears to have over four orders of magnitude of thermal resistance headroom before hitting limits shown for pristine and smooth mechanical contact performance. How much this gap can be closed for standard machined surfaces remains an open question.

The future research in thermal interface materials with ever decreasing size of our electronic devices and components will need to take multi-disciplinary approach. Physics-based model and mechanistic understanding of the problem that the engineers are facing in thermal management of a device/component are essential. In terms of developing new TIMs, the boundary conditions in materials development is required to be set by the reliability engineers and ultimately by the materials/chemical manufacturer for volume production. Understanding of the reliability issues that decipher the degradation trends of the TIMs is yet to be well-understood. Use of eco-friendly materials and processes for the fabrication of next-generation TIMs and understanding of recyclability issues are paramount.

Disclosure statement

No potential conflict of interest was reported by the authors.

Funding

Financial support from European Union's Horizon 2020 TIPS project (the grant agreement No. 644453) is acknowledged. This publication has also emanated from research conducted with the financial support of Science Foundation Ireland (SFI) under [grant number 13/RC/2077].

References

[1] Prasher RS, Koning P, Shipley J, et al. Dependence of thermal conductivity and mechanical rigidity of particle-laden polymeric thermal interface material on particle volume fraction. J Electron Packag. 2003;125(3):386–391.

[2] Xu J, Munari A, Dalton E, et al. Silver nanowire array-polymer composite as thermal interface material. J Appl Phys. 2009;106(12):124310.

[3] Hansson J, Nilsson TMJ, Ye L, et al. Novel nanostruc tured thermal interface materials: a review. Int Mater Rev. 2017, in press.

[4] Due J, Robinson AJ. Reliability of thermal interface materials: a review. Appl Therm Eng. 2013;50 (1):455–463.

[5] McNamara AJ, Joshi Y, Zhang ZM. Characterization of nanostructured thermal interface materials – a review. Int J Therm Sci. 2012;62:2–11.

[6] McWilliams A. Thermal interface materials: technologies, applications and global markets (executive summary), SMC071C, BCC Research; 2015.

[7] Gordon R. Thermal interface materials 2015-2025: status, opportunities, market forecasts (executive summary), IDTechEx; 2016.

[8] http://www.bccresearch.com/market-research/semiconductor-manufacturing/thermal-interface-materials-technologies-applications-global-markets-report-smc071c.html. viewed in 2016.

[9] http://www.bccresearch.com/market-research/semiconductor-manufacturing/the-market-for- thermal-management-technologies-report-smc024k. html. viewed in 2016.

[10] http://www.idtechex.com/research/reports/thermal- interface-materials-2016-2026-status-opportunities- market-forecasts-000474.asp. viewed in 2016.

[11] Xu G. Thermal management for electronic packaging. San Diego (CA): University of California; 2006.

[12] Greenwood JA, Williamson JBP. Contact of nominally flat surfaces. Proc R Soc A: Math Phys Eng Sci. 1966;295(1442):300–319.

[13] Prasher RS. Surface chemistry and characteristics based model for the thermal contact resistance of flu- idic interstitial thermal interface materials. J. Heat Transfer-Trans. ASME. 2001;123(5):969.

[14] Prasher R. Thermal interface materials: historical perspective, status, and future directions. Proc. IEEE. 2006;94(8):1571

[15] Oh BH, Lee EK, Loo HY, et al. The evolution of CPU packaging technology and future challenges. 2006 International Conference on Electronic Materials and Packaging; 2006 Dec 11–14. p. 1-6.

[16] Grujicic M, Zhao CL, Dusel EC. The effect of thermal contact resistance on heat management in the electronic packaging. Appl. Surf. Sci. 2005;246(1–3):290–302.

[17] Mahajan R. Thermal management of CPUs: a perspective on trends, needs and opportunities. Invited Talk Given at the Eighth International Workshop on Thermal Investigations of ICs and Systems (THERMINIC); 2002 Oct 1–4; Madrid, Spain.

[18] Torresola J, Chiu CP, Chrysler G, et al. Density factor approach to representing impact of die power maps on thermal management. IEEE Trans. Adv. Packag. 2005;28(4):659

[19] Chiu C-P. Design and challenges of TIM1 for high-performance microprocessors. Chandler (AZ): Technical Report, Intel Corporation 2006.

[20] Sauciuc I, Prasher R, Chang J-Y, et al. Thermal performance and key challenges for future CPU cooling technologies. ASME Conference Proceedings; San Francisco, California, USA; 2005. p. 353–364.

[21] Rodgers P, Eveloy V, Pecht MG. Extending the limits of air-cooling in microelectronic equipment. Thermal, Mechanical and Multi-physics Simulation and Experiments in Micro-electronics and Micro- Systems, 2005. EuroSimE 2005. Proceedings of the 6th International Conference; Berlin, Germany; 2005. p. 695–702.

[22] Auciello O, Sumant AV. Status review of the science and technology of ultrananocrystalline diamond (UNCD (TM)) films and application to multifunctional devices. Diamond Relat Mater. 2010;19(7– 9):699–718.

[23] Moutanabbir O, Gösele U. Heterogeneous integration of compound semiconductors. Annu Rev Mater Res. 2010;40:469–500.

[24] Hopkins PE. Thermal transport across solid interfaces with nanoscale imperfections: effects of rough- ness. ISRN Mech Eng. 2013;2013:1–19.

[25] Monachon C, Weber L. Influence of diamond surface termination on thermal boundary conductance between Al and diamond. J Appl Phys. 2013;113 (18):183504.

[26] Hohensee GT, Wilson R, Cahill DG. Thermal conductance of metal–diamond interfaces at high pressure. Nat Commun. 2015;6:6578.

[27] Schroeder D, Aksamija Z, Rath A, et al. Thermal resistance of transferred-silicon-nanomembrane interfaces. Phys Rev Lett. 2015;115(25):256101.

[28] Dou R, Ge T, Liu X, et al. Effects of contact pressure, interface temperature, and surface roughness on thermal contact conductance between stainless steel sur- faces under atmosphere condition. Int J Heat Mass Transfer. 2016;94:156–163.

References

[29] Lin YY, Hui CY, Conway HD. A detailed elastic analysis of the flat punch (Tack) test for pressure-sensitive adhesives. J Polym Sci B. 2000;38(21):2769–2784.

[30] Cross GL, O'Connell BS, Pethica JB. Influence of elastic strains on the mask ratio in glassy polymer nanoimprint. Appl Phys Lett. 2005;86(8):81902.

[31] Cross GL. The production of nanostructures by mechanical forming. J Phys D: Appl Phys. 2006;39 (20):R363.

[32] Prasher R. Thermal interface materials: historical perspective, status, and future directions. Proc IEEE. 2006;94(8):1571–1586.

[33] Luo X, Hu R, Liu S, et al. Heat and fluid flow in high-power LED packaging and applications. Prog Energ Combust. 2016;56:1–32.

[34] Prasher RS, Shipley J, Prstic S, et al. Thermal resistance of particle laden polymeric thermal interface materials. J Heat Transfer. 2003;125(6):1170–1177.

[35] Prasher RS. Surface chemistry and characteristics based model for the thermal contact resistance of fluidic interstitial thermal interface materials. J Heat Transfer. 2001;123(5):969–975.

[36] Hamasaiid A, Dargusch MS, Loulou T, et al. A predictive model for the thermal contact resistance at liquid–solid interfaces: analytical developments and validation. Int J Therm Sci. 2011;50(8):1445–1459.

[37] Hamasaiid A, Dour G, Loulou T, et al. A predictive model for the evolution of the thermal conductance at the casting–die interfaces in high pressure die casting. Int J Therm Sci. 2010;49(2):365–372.

[38] Yuan C, Duan B, Li L, et al. An improved model for predicting thermal contact resistance at liquid–solid interface. Int J Heat Mass Transfer. 2015;80:398–406.

[39] Smith B, Glatz W, Michel B. Electronics Cooling Magazine. 2009.

[40] Brunschwiler T, Kloter U, Linderman RJ, et al. Hierarchically nested channels for fast squeezing interfaces with reduced thermal resistance. IEEE Trans Comp Packag Technol. 2007;30(2):226–234.

[41] Bajaj N, Subbarayan G, Garimella SV. Topological design of channels for squeeze flow optimization of thermal interface materials. Int J Heat Mass Transfer. 2012;55(13):3560–3575.

[42] Linderman R, Brunschwiler T, Kloter U, et al. Hierarchical nested surface channels for reduced particle stacking and low-resistance thermal interfaces. Twenty-Third Annual IEEE Semiconductor Thermal Measurement and Management Symposium. San Jose (CA): IEEE; 2007. p. 87–94.

[43] Shirazy MR, Allard S, Beaumier M, et al. Effect of squeezing conditions on the particle distribution and bond line thickness of particle filled polymeric thermal interface materials. Thermal and Thermomechanical Phenomena in Electronic Systems (ITherm), 2014 IEEE Intersociety Conference. Orlando (FL): IEEE; 2014. p. 251–259.

[44] Cooper M, Mikic B, Yovanovich M. Thermal contact conductance. Int J Heat Mass Transfer. 1969;12 (3):279–300.

[45] ASTM. ASTM D5470-12, Standard test method for thermal transmission properties of thermally conductive electrical insulation materials. Vol. 10.02 Electrical Insulation (II): D2518-latest.

[46] Kempers R, Kolodner P, Lyons A, et al. A high-precision apparatus for the characterization of thermal interface materials. Rev Sci Instrum. 2009;80 (9):95111.

[47] Burg BR, Kolly M, Blasakis N, et al. Steady-state low thermal resistance characterization apparatus: the bulk thermal tester. Rev Sci Instrum. 2015;86 (12):124903.

[48] Sponagle B, Groulx D. Measurement of thermal interface conductance at variable clamping pressures using a steady state method. Appl Therm Eng. 2016;96:671– 681.

[49] Zhang P, Xuan Y, Li Q. A high-precision instrumentation of measuring thermal contact resistance using reversible heat flux. Exp Therm Fluid Sci. 2014;54:204–211.

[50] Smith AN, Jankowski NR, Boteler LM. Measurement of high-performance thermal interfaces using a reduced scale steady-state tester and infrared microscopy. J Heat Transfer. 2016;138(4):41301– 41301.

[51] Marconnet AM, Yamamoto N, Panzer MA, et al. Thermal conduction in aligned carbon nanotube–polymer nanocomposites with high packing density. ACS Nano. 2011;5(6):4818–4825.

[52] Barako MT, Gao Y, Won Y, et al. Reactive metal bonding of carbon nanotube arrays for thermal inter- face applications. IEEE Trans Comp Packag Manuf Technol. 2014;4(12):1906–1913.

[53] McNamara AJ, Joshi Y, Zhang Z, et al. Double-sided transferred carbon nanotube arrays for improved thermal interface materials. J Electron Packag. 2015;137(3):31014–31014.

[54] Lee YT, Shanmugan S, Mutharasu D. Thermal resistance of CNTs-based thermal interface material for high power solid state device packages. Appl Phys A. 2014;114(4):1145–1152.

[55] Taylor SH, Garimella SV. Capacitive sensing of local bond layer thickness and coverage in thermal interface materials. Int J Heat Mass Transfer. 2016;97:26–31.

References

[56] Na N, Hasegawa K, Zhou X, et al. Denser and taller carbon nanotube arrays on Cu foils useable as thermal interface materials. Jpn. J. Appl. Phys. 2015;54 (9):95102.

[57] Parker WJ, Jenkins RJ, Butler CP, et al. Flash method of determining thermal diffusivity, heat capacity, and thermal conductivity. J Appl Phys. 1961;32(9):1679–1684.

[58 Khuu V, Osterman M, Bar-Cohen A, et al. Effects of temperature cycling and elevated temperature/humidity on the thermal performance of thermal interface materials. IEEE Trans Device Mater Reliability. 2009;9(3):379–391.

[59] Hone J. Carbon nanotubes: thermal properties. Dekker Encyclopedia Nanosci Nanotechnol. 2004;6:603–610.

[60] Kim P, Shi L, Majumdar A, et al. Thermal transport measurements of individual multiwalled nanotubes. Phys Rev Lett. 2001;87(21):215502.

[61] Yu C, Shi L, Yao Z, et al. Thermal conductance and thermopower of an individual single-wall carbon nanotube. Nano Lett. 2005;5(9):1842–1846.

[62] Peacock MA, Roy CK, Hamilton MC, et al. Characterization of transferred vertically aligned carbon nanotubes arrays as thermal interface materials. Int J Heat Mass Transfer. 2016;97:94–100.

[63] Yao Y, Tey JN, Li Z, et al. High-quality vertically aligned carbon nanotubes for applications as thermal interface materials. IEEE Trans Comp Packag Manuf Technol. 2014;4(2):232–239

[64] Liu J, Jiang D, Fu Y, et al. Carbon nanotubes for electronics manufacturing and packaging: from growth to integration. Adv Manuf. 2013;1(1):13–27.

[65] Xu J, Fisher TS. Enhancement of thermal interface materials with carbon nanotube arrays. Int J Heat Mass Transfer. 2006;49(9–10):1658–1666.

[66] Tong T, Zhao Y, Delzeit L, et al. Dense vertically aligned multiwalled carbon nanotube arrays as thermal interface materials. IEEE Trans Comp Packag Technol. 2007;30(1):92–100

[67] Ganguli S, Sihn S, Roy AK, et al. Metalized nanotube tips improve through thickness thermal conductivity in adhesive joints. J Nanosci Nanotechnol. 2009;9 (3):1727–1733.

[68] Amama PB, Cola BA, Sands TD, et al. Dendrimer-assisted controlled growth of carbon nanotubes for enhanced thermal interface conductance. Nanotechnology. 2007;18(38):385303.

[69] Cola BA, Xu J, Cheng C, et al. Photoacoustic characterization of carbon nanotube array thermal inter- faces. J Appl Phys. 2007;101(5):54313.

[70] Cola BA, Xu X, Fisher TS. Increased real contact in thermal interfaces: a carbon nanotube/foil material. Appl Phys Lett. 2007;90(9):93513.

[71] Ngo Q, Cruden BA, Cassell AM, et al. Thermal interface properties of Cu-filled vertically aligned carbon nanofiber arrays. Nano Lett. 2004;4(12):2403–2407.

[72] Panzer MA, Zhang G, Mann D, et al. Thermal properties of metal-coated vertically aligned single-wall nanotube arrays. J Heat Transfer. 2008;130(5):52401–52401.

[73] Ganguli S, Roy AK, Wheeler R, et al. Superior thermal interface via vertically aligned carbon nanotubes grown on graphite foils. J Mater Res. 2013;28 (07):933–939.

[74] Cola BA, Xu J, Fisher TS. Contact mechanics and thermal conductance of carbon nanotube array interfaces. Int J Heat Mass Transfer. 2009;52(15–16):3490–3503.

[75] Hu XJ, Padilla AA, Xu J, et al. 3-omega measurements of vertically oriented carbon nanotubes on silicon. J Heat Transfer. 2006;128(11):1109–1113.

[76] Gao Y, Marconnet A, Panzer M, et al. Nanostructured interfaces for thermoelectrics. J Electron Mater. 2010;39(9):1456–1462.

[77] Ji Y, Li G, Chang C, et al. Investigation on carbon nanotubes as thermal interface material bonded with liquid metal alloy. J Heat Transfer. 2015;137 (9):91017.

[78] Bar-Cohen A, Matin K, Narumanchi S. Nanothermal interface materials: technology review and recent results. J Electron Packag. 2015;137(4):40803–40803.

[79] John HT, Thomas LB, Virendra S, et al. Carbon nanotube thermal interfaces enhanced with sprayed on nanoscale polymer coatings. Nanotechnology. 2013;24(10):105401.

[80] Qiu L, Wang X, Su G, et al. Remarkably enhanced thermal transport based on a flexible horizontally-aligned carbon nanotube array film. Sci Rep. 2016;6:21014.

[81] Zhong Y, Zhou M, Huang F, et al. Effect of graphene aerogel on thermal behavior of phase change materials for thermal management. Sol Energy Mater Sol Cells. 2013;113:195–200.

[82] Zhang X, Yeung KK, Gao Z, et al. Exceptional thermal interface properties of a three-dimensional graphene foam. Carbon. 2014;66:201–209.

[83] Tang Z, Shen S, Zhuang J, et al. Noble-metal-promoted three-dimensional macroassembly of single-layered graphene oxide. Angew Chem Int Ed. 2010;49(27):4603–4607.

[84] Lv P, Tan X-W, Yu K-H, et al. Super-elastic graphene/carbon nanotube aerogel: a novel thermal interface material with highly thermal transport properties. Carbon. 2016;99:222–228.

References

[85] Liang Q, Yao X, Wang W, et al. A three-dimensional vertically aligned functionalized multilayer graphene architecture: an Approach for graphene-based thermal interfacial materials. ACS Nano. 2011;5 (3):2392–2401.

[86] Sharma M, Chung DDL. Solder–graphite network composite sheets as high-performance thermal interface materials. J Electron Mater. 2015;44(3):929–947.

[87] Warzoha RJ, Zhang D, Feng G, et al. Engineering interfaces in carbon nanostructured mats for the creation of energy efficient thermal interface materials. Carbon. 2013;61:441–457.

[88] Hamdan A, McLanahan A, Richards R, et al. Characterization of a liquid–metal microdroplet thermal interface material. Exp Therm Fluid Sci. 2011;35 (7):1250–1254.

[89] Martin Y, Kessel TV. High performance liquid metal thermal interface for large volume production. IMAPS Thermal and Power Management, San Jose, CA, 2007.

[90] Hill RF, Strader JL. Practical utilization of low melting alloy thermal interface materials. Twenty-Second Annual IEEE Semiconductor Thermal Measurement and Management Symposium; 2006 Mar 14–16. p. 23–27.

[91] Roy CK, Bhavnani S, Hamilton MC, et al. Investigation into the application of low melting temperature alloys as wet thermal interface materials. Int J Heat Mass Transfer. 2015;85:996–1002.

[92] Yang E, Guo H, Guo J, et al. Thermal performance of low-melting-temperature alloy thermal interface materials. Acta Metall Sin (Eng Lett). 2014;27 (2):290–294.

[93] Roy CK, Bhavnani S, Hamilton MC, et al. Thermal performance of low melting temperature alloys at the interface between dissimilar materials. Appl Therm Eng. 2016;99:72–79.

[94] Liu J, Sahaym U, Dutta I, et al. Interfacially engineered liquid-phase-sintered Cu–In composite solders for thermal interface material applications. J Mater Sci. 2014;49(22):7844–7854.

[95] Sharma D, Tiwari RK, Sharma R, et al. Two-phase metallic thermal interface materials processed through liquid phase sintering followed by accumulative roll bonding. IEEE Trans Comp Packag Manuf Technol. 2016;6(1):58–66.

[96] Zhang R, Cai J, Wang Q, et al. Thermal resistance analysis of Sn-Bi solder paste used as thermal interface material for power electronics applications. J Electron Packag. 2014;136(1):11012–11012.

[97] Luo X, Zhang Y, Zandén C, et al. Novel thermal inter- face materials: boron nitride nanofiber and indium composites for electronics heat dissipation applications. J Mater Sci Mater Electron. 2014;25(5):2333–2338.

[98] Raj PM, Gangidi PR, Nataraj N, et al. Coelectrodeposited solder composite films for advanced thermal interface materials. IEEE Trans Comp Packag Manuf Technol. 2013;3(6):989–996

[99] Kempers R, Lyons AM, Robinson AJ. Modeling and experimental characterization of metal microtextured thermal interface materials. J Heat Transfer. 2014;136 (1):11301–11301.

[100] Kempers R, Kerslake S. In situ testing of metal micro-textured thermal interface materials in telecommunications applications. J Phys Conf Ser. 2014;525(1):12016.

[101] Razeeb KM, Roy S. Thermal diffusivity of nonfractal and fractal nickel nanowires J Appl Phys. 2008;103 (8):84302.

[102] Feng B, Faruque F, Bao P, et al. Double-sided tin nanowire arrays for advanced thermal interface materials. Appl Phys Lett. 2013;102(9):93105.

[103] Barako MT, Roy-Panzer S, English TS, et al. Thermal conduction in vertically aligned copper nanowire arrays and composites. ACS Appl Mater Interf. 2015;7(34):19251–19259.

[104] Chen HY, Wei HX, Chen MH, et al. Enhancing the effectiveness of silicone thermal grease by the addition of functionalized carbon nanotubes. Appl Surf Sci. 2013;283(15):525–531.

[105] Kiran CS, Nanda KK. Enhancement of commercially-available thermal grease by multiwalled carbon nanotubes for electronic device applications. Adv Mater Lett. 2013;4(4):22–25.

[106] Zhang P, Li Q, Xuan YM. Thermal contact resistance of epoxy composites incorporated with nano-copper particles and the multi-walled carbon nanotubes. Compos A: Appl Sci Manuf. 2014;57:1–7.

[107] Anithambigai P, Shanmugan S, Mutharasu D, et al. Study on thermal performance of high power LED employing aluminum filled epoxy composite as thermal interface material. Microelectron J. 2014;45 (12):1726–1733.

[108] Shtein M, Nadiv R, Buzaglo M, et al. Thermally conductive graphene-polymer composites: size, percolation, and synergy effects. Chem Mater. 2015;27 (6):2100–2106.

[109] Goyal V, Balandin AA. Thermal properties of the hybrid graphene-metal nano-micro-composites: applications in thermal interface materials. Appl Phys Lett. 2012;100(7):73113.

[110] Yujun G, Zhongliang L, Guangmeng Z, et al. Effects of multi-walled carbon nanotubes addition on thermal properties of thermal grease. Int J Heat Mass Transfer. 2014;74:358–367.

[111] Ahn K, Kim K, Kim J. Thermal conductivity and electric properties of epoxy composites filled with TiO2-coated copper nanowire. Polymer. 2015;76:313–320.

References

[112] Kim CM, Kang YT. Cooling performance enhancement of LED (Light Emitting Diode) using nano- pastes for energy conversion application. Energy. 2014;76:468–476.

[113] Kim K-S, Park B-G, Kim H, et al. Fabrication of Ag-MWNT nanocomposite paste for high-power LED package. Curr Appl Phys. 2015;15:S36–S41.

[114] Raza MA, Westwood AVK, Stirling C, et al. Effect of boron nitride addition on properties of vapour grown carbon nanofiber/rubbery epoxy composites for thermal interface applications. Compos Sci Technol. 2015;120:9–16.

[115] Nakajima A, Shoji A, Yonemori K, et al. Novel polymer composite having diamond particles and boron nitride platelets for thermal management of electric vehicle motors. Jap J Appl Phys. 2016;55(2):27101.

[116] Yu Y-H, Ma C-CM, Teng C-C, et al. Enhanced thermal and mechanical properties of epoxy composites filled with silver nanowires and nanoparticles. J Taiwan Inst Chem Eng. 2013;44(4):654–659.

[117] Wang S, Cheng Y, Wang R, et al. Highly thermal conductive copper nanowire composites with ultralow loading: toward applications as thermal interface materials. ACS Appl Mater Interfaces. 2014;6 (9):6481–6486.

[118] Munari A, Xu J, Dalton E, et al. Metal nanowire-polymer nanocomposite as thermal interface material. 2009 59th Electronic Components and Technology Conference; 2009 May 26–29. p. 448–452.

[119] Razeeb KM, Hasan M, Gautam D, et al. Metallic nanowire-polymer composite as thermal interface material. Meeting Abst. 2014;MA2014-02(36):1862.

[120] Tang B, Hu G, Gao H, et al. Application of graphene as filler to improve thermal transport property of epoxy resin for thermal interface materials. Int J Heat Mass Transfer. 2015;85:420–429.

[121] Shahil KM, Balandin AA. Graphene-multilayer graphene nanocomposites as highly efficient thermal interface materials. Nano Lett. 2012;12(2):861–867.

[122] Jakubinek MB, White MA, Mu M, et al. Temperature dependence of thermal conductivity enhancement in single-walled carbon nanotube/polystyrene composites. Appl Phys Lett. 2010;96(8):83105.

www.nexalus.com

CONTACT US:

Nexalus Ltd,
Unit 13, South Bank,
Crosse's Green,
Cork, Ireland,
T12 XT71

Nexalus Labs,
Water St,
Loughanalla,
Castlepollard,
Co. Westmeath, Ireland,
N91 EP90

Nexalus Research,
Trinity Research & Innovation,
O'Reilly Institute, Trinity College,
Dublin 2, Ireland,

info@nexalus.com
www.nexalus.com

Registered in Ireland No. 628880,
VAT No. IE3573607SH

WITH ENDORSEMENTS AND SUPPORT FROM:

ENTERPRISE IRELAND where innovation means business
Science Foundation Ireland sfi For what's next
Trinity College Dublin Coláiste na Tríonóide, Baile Átha Cliath The University of Dublin
CONNECT
IRISH RESEARCH COUNCIL An Chomhairle um Thaighde in Éirinn

QUALITY CERTIFICATIONS:

IATF 16949 / Automotive Standard
ISO 13485 / Medical Device Standard
ISO 50001 / Energy Management Standard
ISO 45001 / Occupational Heath & Safety Standard
ISO 14001 / Environmental Standard

NEXALUS
COOLING THE CLOUD